frontiers | Frontiers in Environmental Science

TYPE Original Research
PUBLISHED 06 February 2026
DOI 10.3389/fenvs.2026.1736782

OPEN ACCESS

EDITED BY
Sante Laviola,
National Research Council (CNR), Italy

REVIEWED BY
Vincenzo Capozzi,
University of Naples Parthenope, Italy
Francesco De Martin,
University of Bologna, Italy

*CORRESPONDENCE
Susanna Mohr,
susanna.mohr@kit.edu
Mathis Tonn,
mathis.tonn@kit.edu

†These authors have contributed equally to this work and share first authorship

RECEIVED 31 October 2025
REVISED 22 December 2025
ACCEPTED 15 January 2026
PUBLISHED 06 February 2026

CITATION
Mohr S, Tonn M, Augenstein M, Sperka C, Kavil Kambrath G and Kunz M (2026) A 20-year spatio-temporal analysis of 3D radar-based hail tracks in Germany: trends and regional differences.
Front. Environ. Sci. 14:1736782.
doi: 10.3389/fenvs.2026.1736782

A 20-year spatio-temporal analysis of 3D radar-based hail tracks in Germany: trends and regional differences

Susanna Mohr[1,2*†], Mathis Tonn[1*†], Markus Augenstein[1], Christian Sperka[1], Gokul Kavil Kambrath[1] and Michael Kunz[1,2]

[1]Institute of Meteorology and Climate Research Troposphere Research (IMKTRO), Karlsruhe Institute of Technology (KIT), Karlsruhe, Germany, [2]Center for Disaster Management and Risk Reduction Technology (CEDIM), Karlsruhe Institute of Technology (KIT), Karlsruhe, Germany

For a long time, the lack of archived radar data in Germany prevented comprehensive, long-term studies of convective storms. However, the recent availability of a 20-year, homogeneous dataset based on 16, and in some years 17, single-polarization C-band radars now allows for consistent, national-scale analyses. This dataset provides a solid foundation for more precise hail statistical assessments and long-term hail frequency estimation, including potential trends. A tracking algorithm (TRACE3D), which was specifically modified to detect severe convective cells with the potential to produce hail, was used to identify 15,577 potential hail tracks (PHTs) during the summer half-year period from 2005 to 2024. Validation against building insurance data shows that the modified TRACE3D algorithm performs reasonably well and can adequately reproduce hail statistics in Germany. The spatial distribution of the PHTs reveals distinct regional patterns, including a north-to-south gradient influenced by the proximity to seas and orographic features. The highest hail frequency occurs south of Stuttgart and over the Bavarian Prealps. Most tracks are shorter than 40 km and last no more than 75 min (both at the 75th percentile). Nearly 60% of the tracks show a propagation direction from southwest to northeast, which aligns with typical mid-tropospheric conditions favoring convection. Furthermore, half of the days with PHTs are associated with atmospheric blocking regimes, such as Scandinavian, European, or Greenland blocking. Hail events in Germany are unevenly distributed in time. Sixty-three percent of days record no PHTs, and there are only occasional periods of intense hail activity with many tracks per day. While many hail days tend to be isolated (40%), under certain weather conditions, serial clustering of several hail days can form. However, such episodes rarely last more than 2 weeks and are often associated with prolonged blocking. Trend analyses show a high annual variability in PHTs with no clear trend for entire Germany. However, significant regional differences emerge: northern and central Germany show a decreasing tendency in PHT occurrence, whereas southern Germany exhibits a significant increase.

KEYWORDS

3D radar data, clustering, Germany, hail, hail tracks, spatio-temporal features, trends

1 Introduction

Severe hail events, causing billions of euros of damage to buildings, vehicles, infrastructure, and agriculture, are a recurring weather phenomenon in Germany and have been well documented over the last 2 decades (e.g., Kunz et al., 2018; Púčik et al., 2019; Wilhelm et al., 2024; GDV, 2024a). For instance, the Munich hailstorm on 12 July 1984 (Heimann and Kurz, 1985; Höller and Reinhardt, 1986), with hailstones up to 10 cm in diameter, still tops the loss statistics in motor vehicle damage insurance, with 230,000 vehicles damaged and damage costs of 2.9 billion euros (adjusted for inflation to 2023 values; GDV, 2024a; GDV, 2024b). More than 300 injured people required hospital treatment and three people died of shock (SPIEGEL, 1984). While some insurers had already included hail before, this event led others to expand their natural hazard insurance accordingly (Allianz, 2009). Previously, coverage typically included only winter storms (or damage caused by at least Beaufort 8) and fires.

In terms of property damage, the hailstorms of 27–28 July 2013 (known as hailstorm Andreas; Kunz et al., 2018) are considered the costliest hail-related event in Germany. According to the insurance industry's standard 72-h event definition, these storms caused a total of 4.05 billion euros in insured losses (2.6 billion euros in property damage, 1.45 billion euros in motor vehicle damage; GDV, 2024a; GDV, 2024c). A few days later, on 6 August 2013, the largest hailstone ever recorded in Germany was registered in Undingen (14 km south of Reutlingen; see Figure 1) on the Swabian Jura. According to the European Severe Weather Database (ESWD; Dotzek et al., 2009), it reached a maximum diameter of 14.1 cm (Punge and Kunz, 2016).

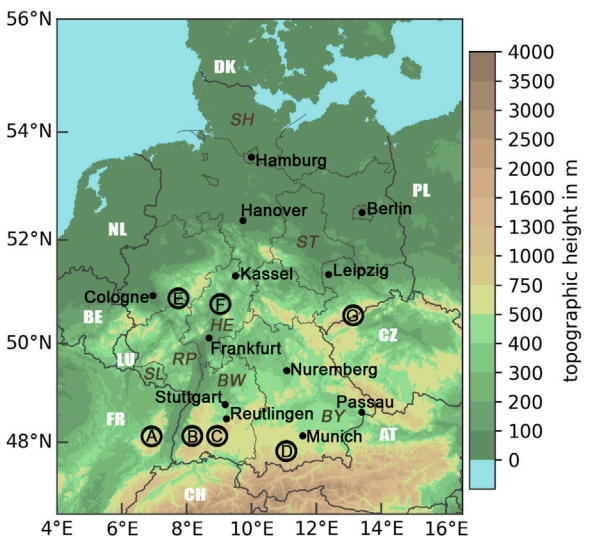

FIGURE 1
Topographic (height) map of the study area, Germany and its neighboring countries: Netherlands (NL), Belgium (BE), Luxembourg (LU), France (FR), Switzerland (CH), Austria (AT), the Czech Republic (CZ), Poland (PL), and Denmark (DK). Various cities and mountain regions (marked in capital letters) are included for orientation: (A) Vosges, (B) Black Forest, (C) Swabian Jura, (D) Bavarian Prealps, (E) Rhenish Mountains, (F) Hessian Highlands, and (G) Ore Mountains. The federal states addressed in the paper are marked with their corresponding abbreviations: Baden-Württemberg (BW), Bavaria (BY), Hesse (HE), Rhineland-Palatinate (RP), Saarland (SL), Saxony-Anhalt (ST), and Schleswig-Holstein (SH).

Despite the wealth of well-documented damage-related events based on claims data from the insurance industry, there is a significant lack of comprehensive, homogeneous long-term hail observations (Martius et al., 2018; Kunz et al., 2025). While some regions of the world (e.g., France and Italy) have operated dense hailpad networks that allow trend estimations (Hermida et al., 2013; Dessens et al., 2015; Manzato et al., 2022), such datasets are not available for Germany.

In contrast, remote sensing products, such as those derived from satellite observations, enable indirect estimation of hail probability on continental or even global scales, either through cloud top features like overshooting tops (OTs; e.g., Bedka, 2011; Mikuš and Mahović, 2013; Punge et al., 2017; Christo et al., 2025) or via passive microwave measurements (e.g., Zipser et al., 2006; Ni et al., 2017; Bang and Cecil, 2019; Laviola et al., 2020). While OTs indicate strong updrafts at the cloud top, often associated with hail-producing storms, microwave sensors supply physical information on frozen hydrometeors inside clouds. Both approaches remain constrained: non-geostationary passive microwave sensors provide only intermittent coverage, and OT analyses suffer from limited spatial resolution and high false positive rates, despite recent improvements (e.g., Bedka et al., 2012; Khlopenkov et al., 2021).

Conversely, radar measurements enable more direct, high-resolution, and temporally continuous observation of precipitation and hail processes, making them the most powerful remote sensing instrument for indirect hail detection (Allen et al., 2020), although this is usually only possible at the national level. In particular, algorithms that analyze volumetric radar reflectivity provide reliable estimates of hail frequency on the ground (e.g., Witt et al., 1998; Delobbe and Holleman, 2006; Kunz and Kugel, 2015; Murillo and Homeyer, 2019). In Germany, radar data have been used for several years to estimate hail occurrence. Kunz and Puskeiler (2010) created the first comprehensive proxy-based hail climatology for southwest Germany (1997–2008) based on the Waldvogel et al. hail criterion (1979). This climatology was developed using three-dimensional (3D) reflectivity from a single-polarization C-band Doppler radar combined with insurance loss data. According to this study, the hail hotspot is located in the Neckar valley downstream of the Black Forest mountains. Building upon this study, Kunz and Kugel (2015) used five established criteria for hail estimation to evaluate the quality of different methods. They found that for the Hail Detection Algorithm (HDA; Smart and Alberty, 1985) and the Probability Of Severe Hail (POSH; Witt et al., 1998) had the highest hail detection skill over a 15-year period, as verified by building insurance data. Puskeiler (2013) and Puskeiler et al. (2016) then applied their findings to 3D reflectivity from the operational radar network of the German Weather Service (Deutscher Wetterdienst, DWD), which at that time consisted of 16 single-polarization C-band radars. The cell tracking algorithm TRACE3D (Handwerker, 2002) was used to estimate individual tracks of convective cells with high reflectivity and, consequently, a high probability of hail on the ground. Their analysis showed that the number of radar-detected hail days increases from north to south. Enhanced hail occurrence is also expected on the leeward side of low mountain ranges. Similar distributions of hail days were also found by

Junghänel et al. (2016) based on the same radar network for the period from 2002 to 2011. However, they used only the precipitation scan at the lowest terrain-following scan level in combination with hail observations from various sources.

Building on the work of Puskeiler (2013), Schmidberger (2018) refined the track identification algorithm to ensure homogeneous tracking and to improve hail detection in a coarse radar dataset (PZ product; see Section 2.1), which is the only product available for a long-term period. Because radar-based methods do not necessarily ensure hail on the ground, the identified tracks are hereinafter referred to as potential hail tracks (PHTs). The PHTs generated with TRACE3D (2005–2015) formed the basis for a stochastically generated event set of hail tracks that is used as input of a hail risk model for building damage. For instance, a simulation period of 10,000 years provided a sufficiently large sample size to estimate the probable maximum loss for a 200-year return period, which is required by insurance industry regulations. This PHT catalog is currently being expanded annually and serves as a basis for addressing additional scientific questions. For example, Kunz et al. (2020) studied the environmental conditions during hail events, particularly in the context of cold fronts and high-shear environments. They found that frontal storm tracks associated with hail produce larger hailstones and longer tracks on average. They also found that deep-layer shear or storm-relative helicity plays an important role in differentiating hail diameter and, in particular, hail track length. In another study (Tonn et al., 2023), the Bunkers' storm motion parameterization of hail-producing supercells (Bunkers et al., 2000), originally developed for the USA, was tested for its applicability in Germany. Due to the different ambient conditions associated with supercells in Europe and the USA (Taszarek et al., 2020a; Taszarek et al., 2020b), adjustments were recommended to improve the estimation of storm motion and to allow more accurate nowcasting of supercell potential. Finally, Li et al. (2025) used the catalog to create and validate a machine learning-based hail prediction model using only convective environmental parameters. The model achieved a Heidke Skill Score of up to 0.66 for areas affected by hail.

With the annual extension of the catalog, PHTs calculated according to the method of Schmidberger (2018) are now available for a 20-year period (2005–2024). This allows more robust analyses of the spatial distribution of hail frequency as well as detailed investigations of their characteristics, such as life cycle or diurnal and annual cycles. Additionally, the 20-year data allow an initial estimation of possible temporal developments and emerging trends.

Therefore, the central research questions of this study are as follows: (i) How reliably can a meaningful proxy-based hail climatology for Germany be derived from 3D radar data using a tracking method for severe convective storms with hail potential? (ii) What is the regional hail frequency across Germany? Which areas constitute hot spots, and which factors explain the observed spatial variability? (iii) What are the average characteristic properties of the PHTs? (iv) Is there evidence of temporal clustering of PHTs? (v) Which large-scale weather patterns favor the occurrence of PHT days? (vi) How have the frequency and characteristics of PHTs in Germany evolved over the past 20 years, and are there spatial differences in these trends?

The paper is structured as follows: Section 2 provides an overview of the datasets and methods used in this study. Section 3 presents the radar-based hail climatology, focusing on the spatial distribution of PHTs and their main characteristics. This includes clustering patterns, such as the daily frequency of PHTs and their occurrence over multiple days. Section 4 investigates trends in PHT's frequency, with a particular focus on regional variations. Finally, Section 5 summarizes the main findings and draws conclusions.

2 Data and methods

Our radar-based hail analysis covers all of Germany (see Figure 1). Neighboring countries and areas over the sea that are partially covered by the DWD radar network were excluded from the analysis. The time period ranges from 2005 to 2024 and covers the months from April to September (summer half-year, SHY), when severe convective storms (SCSs) occur almost exclusively in central Europe (e.g., Wapler, 2013; Punge and Kunz, 2016; Taszarek et al., 2019).

2.1 Radar data

Hail signals were identified from radar reflectivity composites using the operational C-band radar network of the DWD. This network currently consists of 17 weather radars (16 prior to 2013 and between 2018 and 2021; see Supplementary Figure S1 for locations and Supplementary Table S1 for further details in the supplementary material). It is now equipped with the latest dual-polarization Doppler technology. To cover the longest possible period, our study used only single-polarization radar data. Note that the upgrade from single- to dual-polarization radar began in 2011 and concluded in 2021 (Wilke et al., 2025). Although 3D radar data with higher spatial and temporal resolutions, as well as finer intensity classes are now available, we exclusively used the so-called PZ product (single-radar CAPPI reflectivity product) with low resolution (DWD, 2024; DWD, 2025), which has been available since 2005, in order to maintain the comparability and homogeneity of the data basis and to enable consistent statements about temporal trends.

This paragraph describes the main radar specifications that remain the same throughout the study period. A volume scan is performed every 15 min at 18 elevation angles ranging from 0.5° to 37° (Bartels et al., 2005). The scan consists of an intensity mode with a range of 230 km, covering the lowest 4.5°, and a Doppler mode with a range of 120 km, covering all elevations above. The original PZ product derived from this scan has an original spatial resolution of 2 km. For our study, it was resampled to a horizontal resolution of 1×1 km^2 and covers an area of 400×400 km^2 for each radar. It has been available every 15 min since 2005 (since 2013 every 5 min). Radar reflectivity is converted into six discrete reflectivity classes: (7,19], (19,28], (28,37], (37,46], (46,55] and (55,∞) dBZ, at 12 equidistant altitude layers between 1 and 12 km. The two highest classes, (46, 55] and (55,∞) dBZ, are particularly important to our tracking algorithm. Individual PZ volumes were

merged into a radar composite to create the tracks by retaining the highest reflectivity values at overlapping volume points.

Overall, data availability is high, ranging between 87% and 99% depending on the radar location and year. The exception is 2005 with 82.3%, as the PZ product was only available starting in May of that year. Outages due to maintenance and, more importantly, the modernization of the radar network, especially in 2013 and 2014, were compensated for by neighboring radars (backup radars). More detailed information including specific values are listed in the Supplementary Section A1. In the case of radar outages, the composite was constructed using all available radars, partially compensating for spatial gaps through the substantial overlap of the individual PZ volumes (see Supplementary Figure S1). A Doppler filter eliminates ground clutter in the data from fixed objects, mainly at low elevations.

2.2 3D tracking of potential hail-bearing cells

The temporal and spatial evolution of PHTs was tracked by applying an adjusted version of the cell tracking algorithm TRACE3D (Handwerker, 2002) to the 3D radar product. For this purpose, Puskeiler et al. (2016) adapted the algorithm for the binned PZ product in Cartesian coordinates, whereas Handwerker (2002) used single-radar 3D continuous reflectivity in spherical coordinates.

Several radar-based hail studies have used a threshold of 55 dBZ, known as the Mason criterion (Mason, 1971), to detect hail in 2D radar data (Schiesser, 1990; Hohl et al., 2002; Kunz and Kugel, 2015; Junghänel et al., 2016; Fluck et al., 2021). Therefore, identifying potential hail-bearing cells in a PZ composite volume works as follows (see also Schmidberger, 2018): 1. High reflectivity areas were identified by the existence of at least four radar bins of the highest class (55,∞) dBZ. 2. The surrounding (46, 55] dBZ bins were then added to form the so-called reflectivity core (RC). 3. To exclude erroneous radar signals, an RC must have a minimum area of $5 \cdot 10^6$ km^2, and a minimum volume of $3 \cdot 10^9$ km^3, and at least 50% of an RC must extend over two elevation levels.

After detection of potential hail-bearing RCs, their weighted centers were tracked over a constant time interval dt to create PHTs. In the PZ product, dt is 15 min. In this step, TRACE3D attempts to establish a temporal connection between the detected RCs in two time steps. To do so, a 2D shift velocity vector $\mathbf{v}_T$ was calculated for each RC at time t_1. If an RC has already been identified in a previous time step, the shift vector $\mathbf{s}_T$ was computed using the positions at $t_{-1} = t_1 - 2dt$ and $t_0 = t_1 - dt$. If an RC has already been detected in several previous time steps, $\mathbf{v}_T$ was computed as the weighted sum of the velocity vectors from the previous time steps. If an RC is detected for the first time, the shift velocity vector $\mathbf{v}_T$ was estimated from the mean velocity of neighboring RCs. Convective cells are assumed to propagate mainly with the mean wind, which does not exhibit significant spatial variation. The new position of an RC was calculated by $\mathbf{s}_T = \mathbf{v}_T \cdot dt$. Here, the actual RC was identified by searching all possible RCs within a certain radius. The search radius is not fixed; rather, it depends on the distance $\mathbf{s}_T$ and the distance to the nearest neighboring RC. The above-described method was repeated several times for subsequent scans until a complete track of the barycenter of an RC is determined.

Due to the limited number of reflectivity classes available on the equidistant grid, the cells sometimes exhibit only slight differences in their structure. Consequently, TRACE3D may misinterpret the distances and volume structures of potential subsequent cells when linking cells. This incorrect assignment results in an abrupt change in the track direction from one time step to the next. To address this issue, an additional filter criterion has been implemented: a change in track direction of more than 45° with a distance greater than 30 km within 15 min is considered a mismatch and is removed from the dataset. If the mismatch occurs at the beginning or end of a track, the first or last track point is deleted. If the track shift occurs between two RC detections, it was checked to see if two different tracks may be present. This check requires at least three time steps before and after the track shift. Real cell splits and merges, which often involve a significant change in track direction, are unaffected by this correction. Further details on TRACE3D can be found in Handwerker (2002); further details on the adjustment for the PZ product can be found in Schmidberger (2018).

2.3 Potential hail tracks

As described above, the adapted version of TRACE3D was applied to the PZ product (Sect. 2.1) from 2005 to 2024 (SHY) to calculate individual PHTs, which form the basis for the subsequent investigations (PHT catalog). Because a cell lifetime of at least 30 min can be assumed for hailstorms and hail formation (Changnon, 1977; Kumjian et al., 2021), a minimum duration of 45 min, i.e., three time intervals, is required to reconstruct a complete PHT. Additionally, some PHTs are completely outside of mainland Germany because radar data were also available in the surrounding area. Furthermore, some other PHTs extend beyond the border if the cells have formed or dissipated in an adjacent country. However, the dataset only includes PHTs that crossed the German border at some point.

Each PHT contains the following information: start time and lifetime of the cell, cell center at each individual detection (latitude and longitude), total track length (distance between start and end points), mean width (of all RCs relative to the direction of movement), mean direction (angle between start and end points), and mean velocity. Based on the detections of the RCs, polygons with a constant track width perpendicular to the direction of travel were determined (for details, see Section A2 in the supplementary material). For the study, these polygons were gridded at a resolution of 1×1 km^2, forming the basis for further statistical analyses. Some analyses use a coarser grid of 25×25 km^2.

As part of a comparison between the RCs derived from the volume scan of the PZ product and those obtained from a higher-resolved radar product with a 500-m range bin available for a subdomain, it was observed that the widths of the RCs in the previous version of Schmidberger (2018), which were based on the lower-resolved PZ product, were systematically overestimated. This overestimation was largely independent of the size of the associated RCs. Therefore, the width of the RCs derived from the PZ product was adjusted by applying a correction factor of 0.6. A

detailed explanation can be found in the supplement material Section A2.

2.4 Residential building insurance data in Germany

This study uses insurance data to validate the accuracy of the radar-based PHT catalog. The data source is the German Insurance Association (in German: *Gesamtverband der Deutschen Versicherungswirtschaft e. V.*, GDV), an umbrella organization representing all primary insurers in Germany. The data pertain to standard residential building insurance, covering classic risks such as fire, lightning, and water damage, as well as the natural hazards storm and hail (GDV, 2023). The GDV aggregates claims and contract data from all insurers, providing a comprehensive, standardized database. Statistics are available for each of Germany's 400 districts from 2005 to 2023, including the number of daily reported claims and the total annual number of contracts. From these, the claim frequency, i.e., the ratio of reported claims to insured risks (i.e., contracts), is calculated. Setting a threshold allows this measure to serve as an objective indicator of the number of hail days in each district.

Compared to manually collected datasets such as ESWD hail reports, GDV insurance data are more homogeneous, objective, and comprehensive. In 2022, the average insurance density for standard residential building insurance in Germany was about 95% (GDV, 2025). Regional differences are minor: Bavaria has the lowest coverage at 88%, followed by Rhineland-Palatinate (91%) and Hesse (92%). In all other states, coverage is at least 97% (Küpfer, 2025).

Despite its strengths, GDV data are not free of uncertainty. The number of damage reports is particularly influenced by the vulnerability of buildings and the density of buildings in a region. Modern buildings with solar panels, conservatories, or skylights are more susceptible to damage than older buildings (Stucki and Egli, 2007). Additionally, claim dates often differ by ± 1 day from the actual event, because reports are not always assigned precisely. The most restrictive criterion is that the data only includes hail events involving larger, damage-relevant hailstones ($\geq$ 2 cm; e.g., Hohl et al., 2002; Brown et al., 2015; Xiao et al., 2025). A further limitation is that storm and hail claims are recorded jointly, so these damage causes are indistinguishable. Nevertheless, a distinction can be made based on the seasonal distribution of these extremes: storm damage (defined as wind speeds $\geq$ 18 m/s) occurs mainly in winter, while hail damage is almost exclusively reported in summer (Küpfer, 2025). The few summer storm claims usually stem from SCSs with convective gusts or derechos, which often produce hail simultaneously (Pacey et al., 2021). Pure synoptic storms are rare in this season (Mohr et al., 2017).

2.5 Atlantic-European weather regimes

Because SCSs are linked to large-scale atmospheric circulation patterns, we analyzed their relationship with the Atlantic-European weather regimes developed by Grams et al. (2017). These regimes were calculated using the ERA5 reanalysis (Hersbach et al., 2020) from the European Centre for Medium-Range Weather Forecasts (ECMWF) at 12 UTC (Grams et al., 2025; Grams, 2026). The regimes are derived by applying empirical orthogonal functions (EOFs) to mean geopotential height fields (Z500) followed by k-means clustering, yielding seven objectively defined large-scale atmospheric patterns (Grams et al., 2017). Four of these are blocking regimes characterized by positive geopotential height anomalies: Atlantic Ridge (AR), European Blocking (EuBL), Scandinavian Blocking (ScBL), and Greenland Blocking (GL). The regime GL is similar to the negative phase of the North Atlantic Oscillation (NAO; Beerli and Grams, 2019), while EuBL and ScBL represent two variants of the classical blocking pattern (Büeler et al., 2021). The remaining three regimes–the Atlantic Trough (AT), Zonal Regime (ZO), and Scandinavian Trough (ScTr) – are cyclonic regimes with negative geopotential height anomalies and enhanced cyclonic activity. They correlate to varying degrees with the positive NAO phase, with ZO showing the strongest resemblance. An additional "no regime" category is included for days without a dominant large-scale pattern, representing the climatological mean state and capturing transitional or mixed-flow situations. More details are given in Grams et al. (2017) and Büeler et al. (2021).

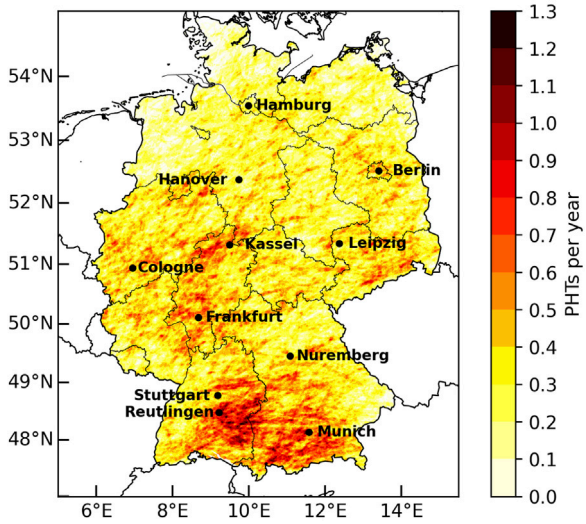

FIGURE 2
Mean annual number of 3D radar-derived potential hail tracks (PHTs) per 1 ×1 km^2 in Germany during the summer half-year (2005–2024). Four grid points reach higher values than 1.3, with a maximum hail occurrence of 1.45 over Germany (all south of Stuttgart).

3 Spatio-temporal radar-based hail statistics

The following sections present the spatial distribution and main characteristics of the PHTs in Germany. TRACE3D (Section 2.2) identified a total of 15,577 PHTs for the SHY period from 2005 to 2024, resulting in an average of approximately 780 PHTs per year. We analyze the spatial and temporal distributions, emphasizing regional hotspots, as well as the primary characteristics of the tracks, including their length, width, duration, and speed.

3.1 Spatial distribution of potential hail tracks

The spatial distribution of days with PHTs in Germany reveals distinct regional patterns, influenced by both climatic and orographic features, as evidenced by the high spatial variability in the mean annual number of PHTs per grid point (Figure 2). The median value for Germany as a whole is 0.3 PHT days per year, with the 25th and 75th percentiles at 0.2 and 0.4, respectively. On the larger scale, a pronounced north-to-south gradient is apparent. In northern Germany, the average is 0.1–0.3 per grid point per year, whereas in southern regions, most values range from 0.3 to 0.6 per grid point per year. A peak of 1.45 occurs near Reutlingen (south of Stuttgart), a well-known hail hotspot in Germany. This large-scale pattern is mainly influenced by the distance to the sea (North Sea and Baltic Sea) and the degree of continentality, which affects the climatological distribution of atmospheric stability in Europe in summer (Mohr and Kunz, 2013; Taszarek et al., 2018; Feldmann et al., 2025b).

In addition, the distribution is shaped by several regional substructures related to orographic features, particularly in mountainous areas and, most notably, downstream of the mountains. For example, pronounced maxima are observed downstream of the Black Forest, over the Swabian Jura and the Bavarian Prealps (see Figure 1, which shows the various low mountain ranges). Supercells with a high potential for large hail are particularly common in the Lech Valley of the Bavarian Prealps (DWD, 2021). Based on high-resolution simulations, Feldmann et al. (2025a) also found an increased frequency of supercells in both the Bavarian Prealps and the lee side of the Black Forest. An increased PHT likelihood is also observed near mountain ranges such as the Ore Mountains, the Hessian Highlands, and the Rhenish Massif. In contrast, some regions in Germany statistically experience fewer than one PHT event every 2 years (84.5% of grid points). The spatial variability of PHT days is primarily driven by flow deviations around orographic obstacles, thermally induced wind systems, and localized convergence of moisture transport (de la Torre et al., 2015; Punge and Kunz, 2016; Allen et al., 2020; Fischer et al., 2025a). Kunz and Puskeiler (2010) and Fluck et al. (2021), for example, hypothesized that the increased hail frequency downstream of the Black Forest (Germany) and the Massif Central (France) is due to relatively high atmospheric instability and low wind speeds in pre-convective conditions. This results in Froude numbers below 1, allowing the air to flow partly around the mountains at low levels. A zone of horizontal flow convergence downstream is created that may initiate convection. The Swabian MOSES field campaign in 2023 (Handwerker et al., 2025) partly confirmed this hypothesis, finding that low-level convergence downstream of the southern Black Forest coincided with convective cell development during several intensive observation periods.

Previous hail statistics for Germany, based on both 2D or 3D radar data, reveal patterns of hail frequency that are similar to those found in our study. This is especially true with regard to the north-to-south distribution of hail frequency and the hotspot regions (Kunz and Puskeiler, 2010; Kunz and Kugel, 2015; Puskeiler, 2013; Puskeiler et al., 2016; Junghänel et al., 2016; Schmidberger, 2018; Fluck et al., 2021; Wilke et al., 2025; Feldmann et al., 2025a). Slight differences in the results are due to several factors: (a) different hail detection methods or criteria, (b) different radar data (2D or 3D, single or dual-polarimetric) and (c) other data sources included (e.g., weather station data, severe weather reports, lightning data). The underlying study periods are usually shorter (maximum 10 years for all of Germany). For example, the most noticeable discrepancy to Wilke et al. (2025) is that the maximum south of Stuttgart is more pronounced in our study than that over the Bavarian Prealps. This difference can primarily be attributed to the different hail detection methods applied by Wilke et al. (2025), who used vertically integrated ice (VII) and maximum estimated size of hail (MESH) derived from radar reflectivity, rather than to the shorter 6-year analysis period (2018–2023; not shown).

3.2 Validation of potential hail tracks against building insurance data

We use categorical verification with a 2 × two contingency table and the GDV insurance data to assess how closely the radar-based hail statistic in Section 3.1, i.e., a proxy derived from remote sensing, aligns with events that occurred. Please note that the insurance data also not fully reflect reality (see Section 2.4). From this table, we compute common skill metrics (Wilks, 2006): the Probability of Detection (POD), measuring the share of correctly forecasted events; the False Alarm Ratio (FAR), indicating incorrect forecasts; and the Heidke Skill Score (HSS; Heidke, 1926), a normalized measure accounting for chance agreement. Ideally, POD and HSS would be close to one, reflecting perfect detection and maximum skill, while FAR would approach zero, indicating an absence of false alarms.

The verification period spans from May 2005 to August 2023, when both datasets are available. To avoid potential storm damage reports in April or September (see Section 2.4), the validation only considers the four summer months most relevant to hail: May, June, July, and August (see Section 3.3). The maximum spatial allocation distance is 20 km between a track and an affected district. An insurance-based hail day is defined by two thresholds, derived from sensitivity analyses that improve the HSS results: at least five claims per district per day (to filter out days with too few reports, especially in small counties with few contracts) and a claim frequency of 0.0001 (to exclude an excessive number of false reports in densely populated regions such as Berlin or Hamburg). Both thresholds address different distortions and help prevent misclassifications caused, for example, by incorrect time allocation.

The evaluation shows that the modified TRACE3D algorithm (Section 2.2) can essentially reproduce hail statistics in Germany (Figure 3). For the entire study area, the results yield a median HSS value of 0.47, with an interquartile range of 0.41–0.52 (25th/75th percentiles). The corresponding POD values are 0.43, ranging from 0.35 to 0.51 (25th/75th percentiles), while the FAR values are 0.36, ranging from 0.27 to 0.49 (25th/75th percentiles). The latter demonstrates that many tracks occur without any associated claim reports. However, this does not necessarily mean that the method is flawed. It may instead indicate that the hail was small and therefore did not cause any damage. Note that the TRACE3D-based algorithm was originally designed to detect hail in general (cf. Puskeiler et al., 2016; Schmidberger, 2018), including smaller events. For this purpose, the original calibration used insurance data from the agricultural sector, in which hailstones larger than 5 mm are considered relevant in terms of causing damage.

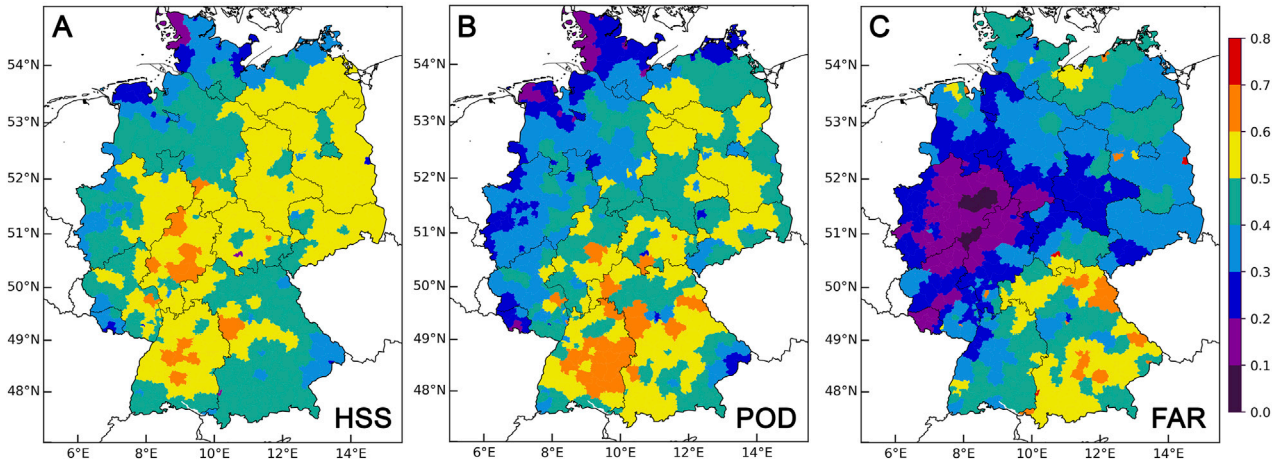

FIGURE 3
Validation of radar-based potential hail tracks (PHTs) using the standard residential building insurance data from the GDV based on the following metrics: **(A)** Heidke Skill Score (HSS), **(B)** Probability of Detection (POD), and **(C)** False Alarm Ratio (FAR) for the period May 2005 to August 2023.

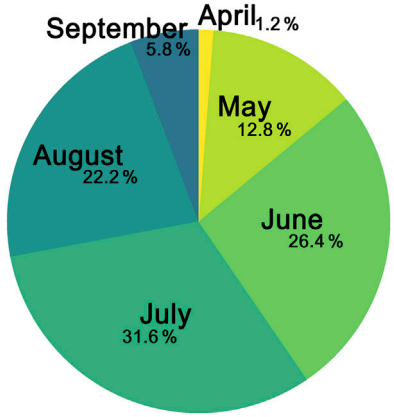

FIGURE 4
Monthly distribution of all 15,577 potential hail tracks (PHTs) from 2005 to 2024.

Moreover, regional differences exist. Good HSS values between 0.5 and 0.7 are found in southern, central, and eastern Germany (Figure 3A). The best performance is found in Saxony-Anhalt (median: 0.55, 25th/75th percentiles: 0.52–0.57), Hesse (median: 0.54, 25th/75th percentiles: 0.50–5.55), and Baden-Württemberg (median: 0.52, 25th/75th percentiles: 0.49–0.58). Lower accuracy appears near some state borders, for example, in the eastern corner of Bavaria (near Passau; see Figure 1) and in Saarland, mainly due to limited radar coverage and outages (see supplementary material Section A1). Skills are also reduced in western North Germany, especially Schleswig-Holstein, which has the lowest median HSS value of 0.31 (25th/75th percentiles: 0.25–0.39). In addition to the issue of radar availability, this could also be due to the fact that the GDV data in this region considers storm damage in some cases. Due to their proximity to the sea, these areas are more exposed to such events. Despite the inherent uncertainties in both datasets, the calculated metrics yield results comparable to those of other studies (e.g., López and Sánchez, 2009; Kunz and Kugel, 2015; Puskeiler et al., 2016; Voormansik et al., 2017; Schmidberger, 2018; Kopp et al., 2024). Overall, these findings underscore the reliability of the modified TRACE3D algorithm in reproducing radar-based hail statistics in Germany, establishing a solid basis for subsequent evaluations.

3.3 Spatio-temporal characteristics of potential hail tracks

An analysis of the temporal distribution of the PHT catalog reveals clear seasonal patterns and a preference for specific months of the year (Figure 4). Most of the PHTs occurred in the warm summer season, with a peak in July (31.6%), followed by June (26.4%), August (22.2%), and May (12.8%). Only a small proportion occurred in April (1.2%) and September (5.8%). Almost half of the PHTs (43.1%) reached the detection threshold of 55 dBZ between 13 and 17 UTC (not shown). In general, these temporal patterns align well with the findings of previous studies in Germany (e.g., Schmidberger, 2018; Fluck et al., 2021) and fit into the European context: The hail season generally begins in April/May and ends in August/September (Punge and Kunz, 2016). However, there are regional differences in the main peaks: in central Europe, France, the Alps, and the Po Valley, hail activity is mainly concentrated from June to August. In contrast, in the Mediterranean region (from Spain to Turkey), the highest frequency generally occurs in autumn (Punge and Kunz, 2016; Laviola et al., 2022).

Most of the PHTs are shorter than 50 km (Figure 5A), with a median length of 24.0 km, while the 25th and 75th percentiles are 15.5 and 39.4 km, respectively. In terms of width, the tracks typically measure 3.2 km on average (median), ranging from 2.2 to 4.7 km (25th/75th percentiles; Figure 5B). The PHTs persist on average about 60 min, with durations ranging between 45 and 75 min (25th/75th percentiles; Figure 5C). The statistical characteristic of the mean track speed per cell is 33.0 km h^{-1} on average (median), ranging from 21.7 to 46.4 km h^{-1} (25th/75th percentiles; Figure 5D).

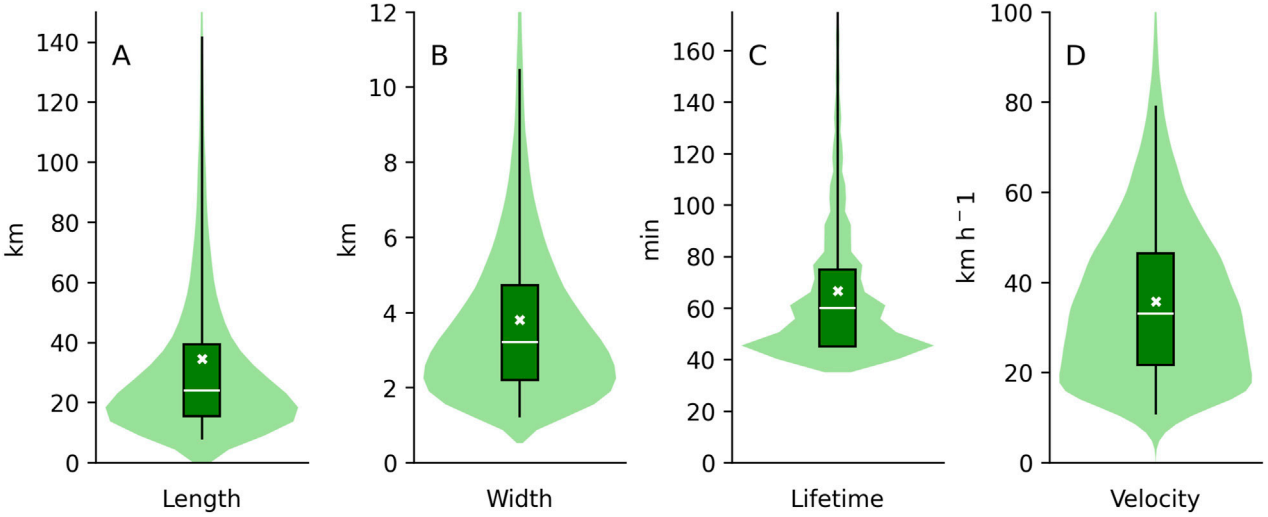

FIGURE 5
Frequency distributions of various potential hail track characteristics (total number: 15,577 PHTs, 2005–2024, SHY): **(A)** Track length in km, **(B)** track width in km, **(C)** track lifetime in min (15 min resolution), **(D)** mean track speed in km h^{-1}. The interquartile range is represented by the boxes, the median by the white line, and the mean by the white cross. Whiskers display the 2nd and 98th percentiles. Few events exceed the shown range of values. Maxima for the respective characteristics are: **(A)** 446 km, **(B)** 34 km, and **(C)** 525 min.

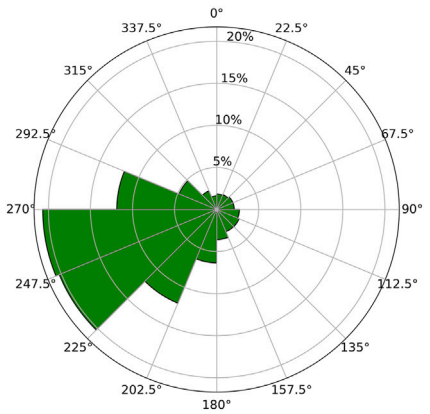

FIGURE 6
Frequency distribution of track motion direction in ° for all 15,577 PHTs (2005–2024, SHY).

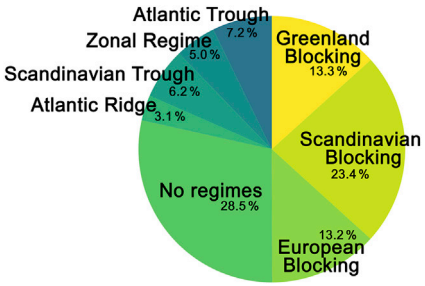

FIGURE 7
Distribution of the PHT days occurring under the different Atlantic-European weather regimes (2005–2024, SHY), using the regime classification of Grams et al. (2017).

Note that in environments with many convective cells, links between consecutive time steps can influence the calculated track speed if the algorithm jumps between neighboring cell cores. Such jumps, which may occur on days with a high density of closely spaced cells (e.g., in mesoscale convective systems), can artificially increase the recorded displacement. Even though the track still represents an area potentially affected by hail, these jumps can lead to an overestimation of track speed. For this reason, we have not specified a maximum value for track speed (as it was observed especially at the upper end of the distribution). On average, however, the values remain realistic, as confirmed by plausibility checks.

Figure 6 clearly illustrates that the majority of tracks propagate from southwest to northeast (53% PHTs are between 202.5° and 270.0°). This aligns with various studies on SCSs that link heavy rain or hail events in central Europe with mid-tropospheric flow characteristics (e.g., Wapler and James, 2015; Piper et al., 2019; Merino et al., 2019; Whitford et al., 2024), which in turn influence the movement direction of the associated cells. Additionally, the advection of warm, moist and thus often unstable air masses from the south and southwest is well-known to create optimal settings for convection-favoring conditions over western and central Europe (van Delden, 2001; Mohr et al., 2019; Barras et al., 2021).

These findings are further supported when the analyses are combined with large-scale weather patterns such as the Atlantic-European weather regimes according to Grams et al. (2017). The results (Figure 7) show that half (50.0%) of days with PHTs are primarily associated with the three blocking regimes: Scandinavian Blocking (23.4%), European Blocking (13.2%), and Greenland Blocking (13.3%). All of these regimes support the convection-favoring large-scale atmospheric condition with a south-to-southwesterly mid-tropospheric flow direction over central

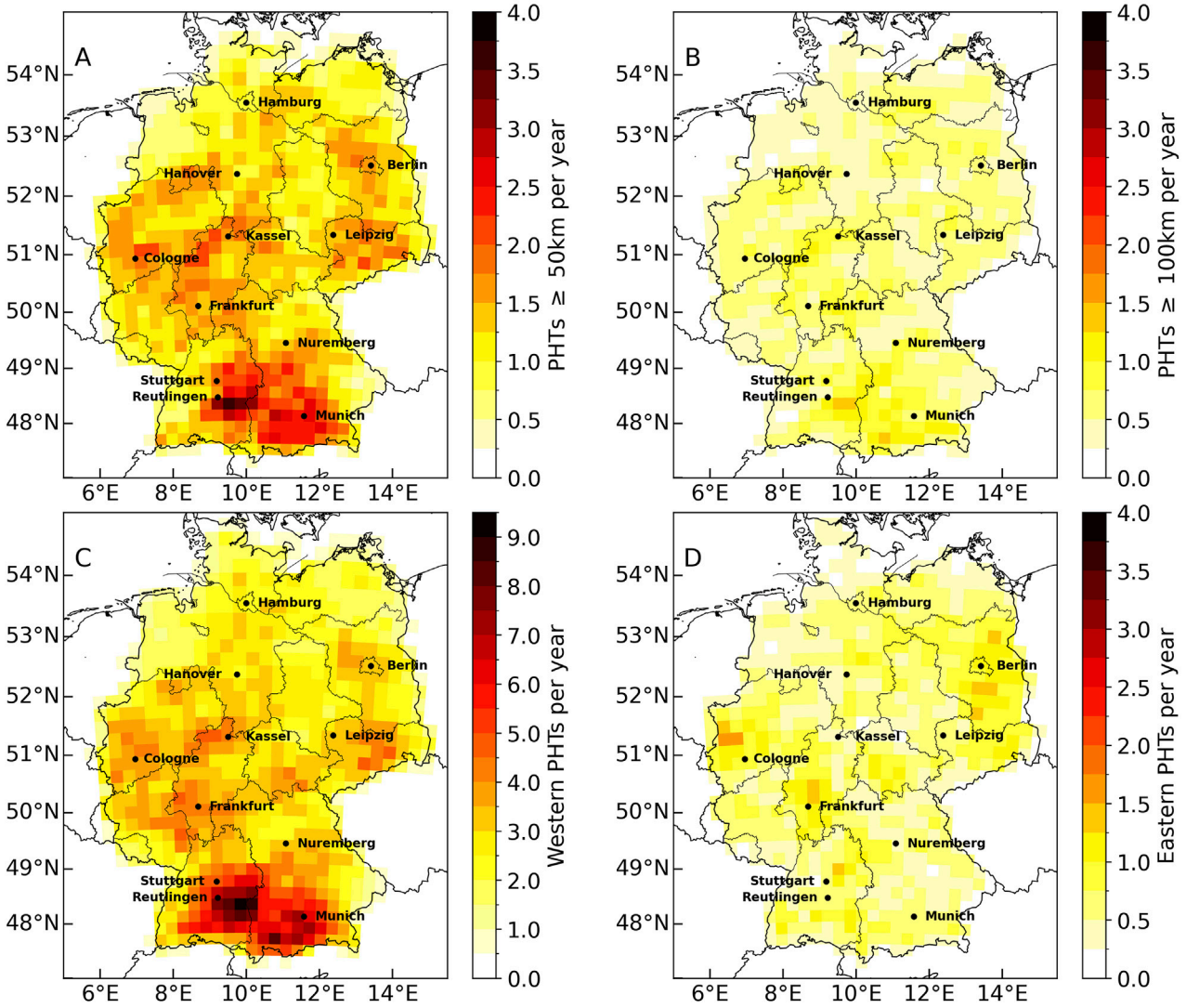

FIGURE 8
Mean annual number of 3D radar-derived potential hail tracks (PHTs; SHY, 2005–2024) per 25 × 25 km² area, categorized by specific characteristics: **(A)** Tracks with a minimum length of 50 km, **(B)** tracks with a minimum length of 100 km, **(C)** tracks originating from the west (between 180° and 360°) and **(D)** tracks originating from the east (between 0° and 180°). Note: Plot **(C)** uses a different color scale.

Europe. In contrast, the remaining four regimes play a minor role (21.5%): Atlantic Trough (7.2%), Atlantic Ridge (3.1%), Zonal Regime (5.0%), and Scandinavian Trough (6.2%). Days without a clearly defined regime (so-called no regime), representing the climatological mean, account for about 28.5%. Similar relationships between these weather regimes and SCSs in general have already been observed in central Europe (Mohr et al., 2019; Augenstein, 2025). Overall, this indicates that PHTs occurred predominantly under blocking regimes (50%) or during periods without a clearly defined large-scale flow pattern ("no regime"), together accounting for approximately 80% of all PHT days.

To study the spatial variability of events with different characteristics, the PHT catalog was aggregated onto a coarser 25 × 25 km² grid, ensuring a sufficient number of events in all grid points. Considering only PHTs of at least 50 km (approximately the 83rd percentile of the track length distribution), the spatial distribution of the PHTs (Figure 8A) remains similar to that of all tracks (Figure 2), although only 17.0% of all tracks reach this length. Nevertheless, a conspicuous maximum is visible southeast of Reutlingen with almost four events per grid point. Higher values also occur in southern Bavaria around Munich, as well as in the area between Frankfurt, Kassel, and Cologne. PHTs reaching 100 km in length are rare, accounting for only 5.0% of all PHTs, which results in fewer events per grid point (Figure 8B). In the same areas, maxima of approximately 1.5 PHTs per year are observed, but differences compared to the surrounding regions are minor. In the end, this highlights that long hail tracks can occur across all parts of Germany.

In order to examine whether the results in Figure 6 show a uniform distribution across Germany or if regional differences exist, PHTs with a direction between 0° and 180° were defined in this study as eastern tracks, and those between 180° and 360° as western tracks. As shown in Figure 6, western tracks dominate the dataset (80.0%). The spatial distribution of the annual number of hail events with western directions (Figure 8C) is close to that of all tracks, with

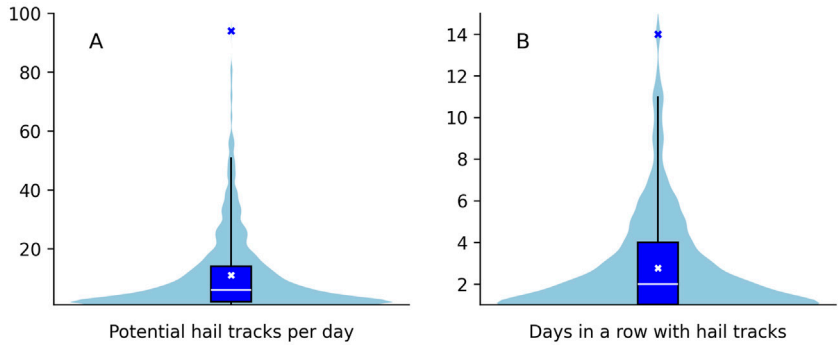

FIGURE 9
(A) Frequency of potential hail tracks (PHTs) per day across Germany. **(B)** Clustering of PHTs over consecutive days across Germany. The box represents the interquartile range, while the whiskers indicate the 2nd and 98th percentiles. The median is shown as a white line, the mean as a white cross, and the maximum value as a blue cross. Light blue shadings represent the probability distribution of the respective variable.

a clear maximum of more than nine events southeast of Reutlingen. High values also occur in the Bavarian Prealps. The strong maximum over the Swabian Jura supports the hypothesis of flow convergence in this zone for (south)westerly flow directions (see Section 3.1). In contrast, the distribution of eastern tracks (20.0%) shows different patterns (Figure 8D): No maxima are found over southern Germany. The highest numbers, with values below two PHTs per year, occur in eastern Germany, north of Frankfurt, and north of Cologne. Overall, the number of eastern tracks is significantly smaller than that of western tracks. The small regional variations suggest a more uniform spatial distribution across Germany.

3.4 Clustering characteristics of potential hail tracks

Investigating the temporal clustering of extreme events, which can often be linked to persistent large-scale weather patterns, is also relevant, as periods with repeated occurrences (compound events) can lead to cumulative impacts (e.g., Zscheischler et al., 2020; Xoplaki et al., 2025; Küpfer et al., 2025). The following analysis examines whether days with detected PHTs cluster in time, either on the daily scale (spatial clustering) or with respect to their persistence across consecutive days (serial clustering). On a daily scale, 61.3% of all days in the study period had no PHTs across Germany (not shown). Of the remaining days with at least one PHT, most contain only a few tracks (Figure 9A): 28.5% show one or two PHTs, about half (47.2%) have up to five, and roughly 65% have no more than 10 tracks. However, there are also some days with significantly higher amounts. For instance, on 30 May 2017, a record of 94 PHTs occurred over large parts of Germany. Additionally, some other days feature a substantial number of PHTs. Approximately 2.4% of all days with tracks have at least 50 PHTs per day. Most of these days fall in June and July.

The serial clustering can provide information about the persistence of the underlying atmospheric conditions and thus also about an ongoing hazard. As with the PHT amounts per day (above), the following statistics refer to the whole of Germany. Therefore, two consecutive hail days do not mean that a particular location was hit by potential hail twice, only that a potential hailstorm occurred somewhere in Germany on both days. In extreme cases, this could mean that 1 day, a PHT occurred in the far north of Germany, and the next day, it occurred in the far south. Of the days with at least one PHT, 41.6% appear isolated (Figure 9B), meaning that the day before and the day after have no PHT anywhere across Germany. In 20.8% of the cases, two consecutive days have at least one PHT, in 12.0% they have three consecutive days. Longer continuous periods are uncommon, as a single day without PHTs resets the count. The longest continuous period with PHTs was 14 days, and this was observed three times during the 20-year study period. Notably, two of these episodes occurred in quick succession with only a brief interruption, spanning from 18 June to 1 July 2021 and from 4 July to 17 July 2021. Both periods were accompanied by different blocking regimes (cf. Kunz et al., 2022). Initially, there were 4 days with no regime, followed by a prolonged blocking phase. During this phase, the atmospheric circulation alternated between European blocking, Scandinavian blocking, and then European blocking again. The third 14-day period occurred from 26 May to 8 June 2016, when atmospheric blocking caused also favorable convective conditions over 2 weeks (cf. Piper et al., 2016).

4 Trends of potential hail tracks

Although a 20-year period is considered relatively short for in-depth trend analysis, the dataset offers a valuable basis for initial estimates. These results should still be interpreted with caution, but they can help to identify early signals of shifts in hail frequency. To examine trends in PHTs, we counted the number of PHTs occurring over Germany during each of the 20 years (SHY; Figure 10). There is a significant year-to-year variability, with more than 1,000 PHTs in 2006, 2014, and 2017, compared to only about 500 in 2010, 2013, and 2023. As shown in the supplementary material (Supplementary Figure S4), the high annual variability is also clearly visible in the annual spatial distribution of the total number of PHTs. These findings are consistent with previous studies (e.g., Mohr et al., 2015; Madonna et al., 2018; Wilhelm et al., 2024). Overall, the time series shows no clear, statistically significant trend. A similar analysis using

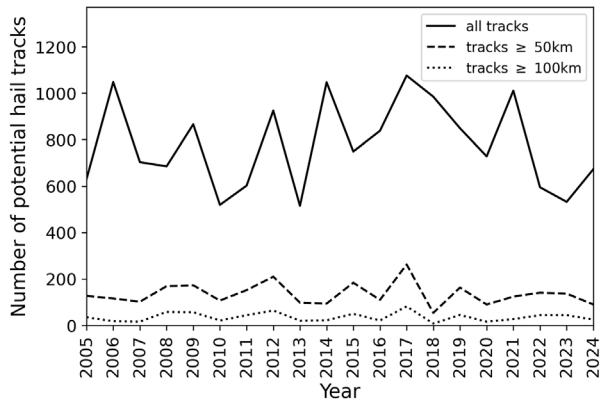

FIGURE 10
Time series of the annual total number of potential hail tracks (PHTs) across Germany (2005–2024, SHY). Different line types represent all tracks (solid) and those with a specific minimum length (dashed: 50 km, dotted: 100 km).

only PHTs longer than 50 and 100 km also reveals substantial year-to-year variability, but no discernible trends.

Although no nationwide trend is apparent, the question remains if there are regional differences. Previous studies on SCSs (western and central Europe; Augenstein et al., 2025), hail (Canada; Cao, 2025), and tornadoes (United States; Graber et al., 2024) have shown that geographically resolved analyses can reveal deviations from the overall, averaged trend. For analyzing regional differences, the PHT catalog is used on a 25 km × 25 km grid to ensure a solid database for each grid point. This provides each grid point with a time series similar to that in Figure 10. The trend is analyzed using the non-parametric method of the repeated median estimator (Siegel, 1982). One advantage of such a non-parametric test is its robustness to outliers (Lanzante, 1996). After trend-free prewhitening of the time series (Yue et al., 2002), the Mann-Kendall test is used to calculate the significance of the trends (Mann, 1945; Kendall and Gibbons, 1955). This approach has already been applied in previous studies to reduce autocorrelation and increase test power (e.g., Mohr and Kunz, 2013; Augenstein et al., 2025; Cao, 2025).

Trend analysis using the repeated mean estimator reveals clear regional differences. Across northern and central Germany–basically excluding the southern federal states of Baden-Württemberg and Bavaria–several grid points show no or only slight negative trends of mostly minus two to minus three events per decade over the 20-year period (Figure 11A). According to the Mann-Kendall test, some of the negative trends in the Cologne, Hamburg, and Berlin regions are statistically significant. The strongest negative trends indicate a reduction of around four events per decade east of Frankfurt. In contrast, southern Germany experiences an increase in PHTs. The most pronounced and also significant increases occur along the Bavarian Prealps and slightly south of the hail hotspot identified in Figure 2, southeast of Reutlingen, with up to ten additional events per decade. Note that on 3 April 2013, the DWD put an additional radar into operation near Memmingen (marked by a black cross in Figure 11A). The improved radar coverage in southern Germany may have contributed to the observed positive trends in this area. However, considering only the trends of the 12 years since installation, the trends remain positive but with less significance for this shorter time period (not shown).

As a minimum length of 100 km yields too few events for reliable trend analysis (see Figure 10), we concentrate in the following only on PHTs of at least 50 km (Figure 11B). No trend can be observed at many grid points, although a tendency toward similar spatial trend patterns can be seen. For example, some grid points in central and northern Germany exhibit negative trends, whereas those in the south exhibit positive ones. However, these trends are less pronounced overall. Additionally, the smaller dataset significantly reduces statistical significance.

When the PHTs are split by direction (analog to Figures 8C,D), the trends for the western tracks (Figure 11C) are very similar to those of all tracks (Figure 11A). This is consistent with the fact that the majority of the tracks originate from the western sector (i.e., 180 to 360°; Figure 6). Conversely, there are only 20% of all PHTs with eastern direction (i.e., 0 to 180°). These fewer events are more equally distributed, so that virtually no trends can be observed (only 6 of 727 grid points over Germany with a slight but insignificant trend) (Figure 11D).

Despite the limited database spanning only 2 decades, the results show clear, statistically significant patterns that extend over larger contiguous areas and thus are not merely isolated outliers. The decrease across parts of central and northern Germany is also consistent with the findings of Augenstein et al. (2025), who based their analysis on lightning data from 2001 to 2021 and likewise observed a decline in SCS frequency. This agreement is particularly noteworthy because the latter study relies on direct observational data. Other studies report other signals for Germany and surrounding European regions and often refer to an increase in hail occurrence. However, these findings are primarily derived from statistical modeling with hail-relevant parameters (ingredients-based forecasting; Mohr et al., 2015; Rädler et al., 2018; Taszarek et al., 2021; Battaglioli et al., 2023) rather than direct observational data. As already cited in Raupach et al. (2021), earlier hail observations in Europe, including Germany, show heterogeneous signals. For example, there is an increasing trend in parts of central and western Europe, including southwestern Germany and Switzerland, while there are decreasing or insignificant trends further south and east. These regional differences in historical hail activity underscore the need for more in-depth research to better understand the complex processes involved in hail formation. Such an understanding is also essential for evaluating the effects of climate change on the frequency and intensity of hail events, as well as for identifying factors that will significantly impact their future occurrence and severity.

Finally, it should be noted that radar failures may have potentially influenced the results. However, as mentioned above, the data availability is generally good at around 90%, and many areas are also covered by multiple radar systems (see the supplementary material Section A1 for details). Sensitivity studies were also conducted to verify the robustness of the trend analyses. Individual data points were systematically excluded using bootstrap approaches (by randomly removing between 5 and 20% of the PHTs), as well as entire years or different subperiods. These tests allowed us to evaluate the sensitivity of the results to random data gaps, targeted failures in specific years, and shortened

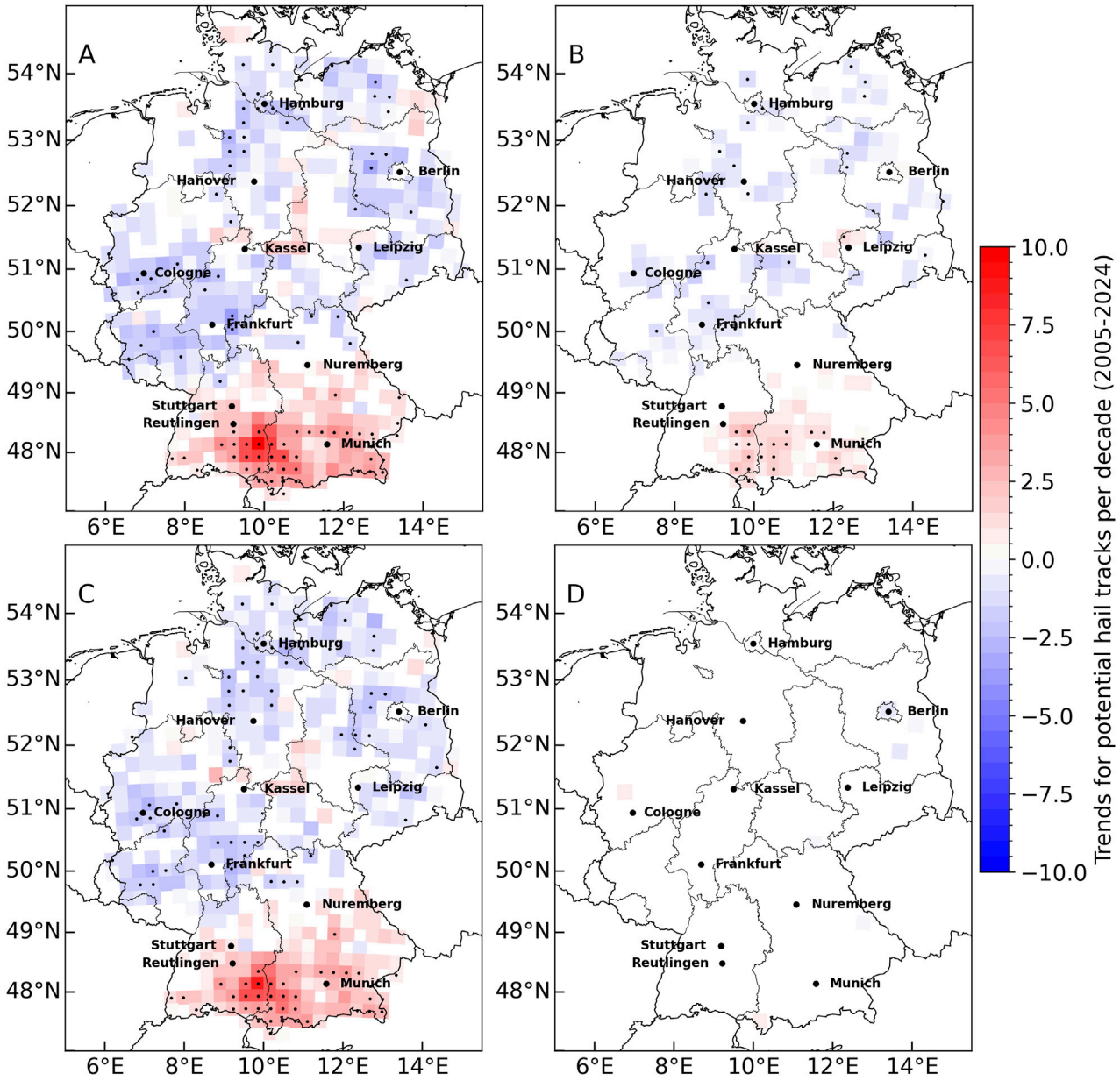

FIGURE 11
Spatially resolved trends (per decade) of potential hail tracks (PHTs, 2005–2024, SHY) per 25 × 25 km^2: **(A)** All PHTs across Germany, **(B)** PHTs with a minimum length of 50 km, **(C)** tracks originating from the west (between 180° and 360°) and **(D)** tracks originating from the east (between 0° and 180°). Small points indicate statistical significance at the 0.05 level according to the Mann-Kendall test (trend-free prewhitening). The black cross in **(A)** marks the location of the Memmingen radar, operational since April 2013.

time series. The analyses confirm the stability of the identified trend tendencies.

5 Discussion and conclusion

Severe convective cells with the potential to produce hail events in Germany were analyzed using 3D radar composites, consisting mainly of 16, and in some years also 17, single-polarized C-band radars from the DWD. A modified version of the TRACE3D tracking algorithm was used to identify the cells. Handwerker (2002) originally developed this algorithm, which was later optimized by Schmidberger (2018) for detecting hail events. Additionally, Schmidberger adapted the algorithm to the coarse spatial and temporal resolution of the DWD radar product (PZ product), which has a temporal resolution of 15 min, 12 elevation levels, and six discrete reflectivity classes. However, because radar-based methods do not necessarily guarantee hail occurrence on the ground, the identified tracks are referred to as potential hail tracks (PHTs) in this study. The dataset has since been updated annually and is now available for a 20-year period.

A total of 15,577 PHTs were identified for the summer half-year from 2005 to 2024. This dataset enables consistent assessment of

spatial and temporal hail patterns, as well as regional trends. The results show clear spatial and temporal structures. Our study is the first to estimate nationwide hail frequency over 2 decades based on a homogeneous 3D radar composite.

The main conclusions from our research are the following:

- Using building insurance data to validate radar-based PHTs reveals an average Heidke Skill Score (HSS) of 0.5 for Germany, with some regions reaching between 0.6 and 0.7. This confirm that the modified TRACE3D algorithm can accurately reproduce hail statistics, showing acceptable, though not exceptional, reliability. Regional skill differences stem from limited radar coverage (e.g., at state borders) and uncertainties in the GDV data (e.g., inaccurate time specifications). Additionally, since the validation data includes only events that caused damage, weak hailstorms with small hailstones are underrepresented.
- Hail hazard across Germany varies significantly due to the influence of regional orography and large-scale patterns, such as those influenced by the proximity to seas and continentality. The highest frequency of radar-identified hail days occurs over southern Germany and downstream of low mountain ranges. The 20-year, radar-based hail climatology generally aligns with prior climatologies that used shorter time windows (e.g., 7 and 11 years, respectively, in Puskeiler et al., 2016; Schmidberger, 2018) or 2D radar data (Junghänel et al., 2016; Fluck et al., 2021).
- Most PHTs propagate from southwest to northeast. They have a median length of 24 km, a median width of 3.2 km, and a median propagation speed of 33 km h^{-1}, which is consistent with earlier studies (Schmidberger, 2018).
- Hail in Germany is usually sporadic, but frequently clusters under favorable large-scale flow conditions. Half of all PHT days occur during blocking regimes. While approximately 42% of PHT days are isolated, 2–3-day clusters are common, and rare persistent episodes can last up to 2 weeks during prolonged blocking. Spatial clustering also occurs, with one-third of hail days featuring more than ten PHTs. Blocking regimes create conditions that favor convection and sustain multi-day hail hazards, so large-scale circulation should be considered alongside local thermodynamic and dynamic indices for forecasting and risk assessment.
- During the past 20 years, the estimated hail hazard from PHTs has remained consistent over the entire Germany. However, disparate trends emerge when examining the data regionally: Southern hotspots, particularly near Reutlingen and the Bavarian Prealps, show statistically significant increases in PHTs, which persist for longer tracks and westward-moving events. Meanwhile, there is a tendency toward a decline in PHTs occurring in northern and central Germany. This finding is somewhat surprising because it contradicts the widely accepted assumption that an increase in temperature and moisture leads to more SCS. However, it aligns with Manzato et al. (2025), who also found negative trends in hail observations in northeastern Italy that differ from those expected from convective variables.

Although the 20-year radar dataset used here is longer than in previous hail studies (e.g., Puskeiler et al., 2016; Junghänel et al., 2016; Nisi et al., 2018; Wilke et al., 2025), it is still relatively short for robust trend estimation. Therefore, the signals found should be interpreted as an indication of potential changes in hail frequency rather than as definitive evidence. Interestingly, parallel studies also show negative trends in convective activity, as evidenced by the rate of lightning over northern Germany (Augenstein et al., 2025). In the coming years, existing analyses can be continuously expanded to verify the robustness of the trends and rule out possible distortions due to short data segments.

The central open question is which physical processes control the regionally different trends in PHTs and which meteorological (e.g., internal climate variability) or anthropogenic factors underlie this pattern. Hail formation is a highly complex interaction of several processes (instability, moisture advection, orographic influences, synoptic regimes, and convective dynamics; cf. Allen et al., 2020), which makes it difficult to clearly assign specific causes. Furthermore, large uncertainties remain in how the response of large-scale atmospheric dynamics (e.g., prevailing weather regimes) and the associated environmental conditions, as well as kinematic aspects (e.g., updraft width and strength of supercells, cf. Fischer et al., 2025b) will respond to a warming climate. The same applies to the response of microphysical processes (e.g., aerosol concentrations; cf. Raupach et al., 2021; Brennan and Wilhelm, 2025). Initial results indicate that the observed trends cannot be attributed solely to changes in large-scale environmental conditions such as atmospheric stability, moisture advection in the lower layers, vertical shear, the melting layer, or the frequency of favorable synoptic configurations. Recent analyses reveal that several factors are operating simultaneously, including teleconnection influences, variations in aerosol concentrations, and alterations in the type and dynamics of thunderstorm systems (e.g., Augenstein et al., 2025; Fischer et al., 2025b; Feldmann et al., 2025a; Manzato et al., 2025; Sperka et al., 2025; Trapp et al., 2025).

A potential limitation of this study is its reliance on the PZ product, which has relatively low vertical resolution and only six reflectivity classes. Nevertheless, this dataset is the only 3D hail-proxy product available consistently over a 20-year period. However, preliminary analyses based on the 2D precipitation scan from DWD with practically continuous scale (RX product, >55 dBZ) reveal similar spatial patterns.

In this work, we have refrained from combining our PHTs with hailstone size data (e.g., ESWD or crowdsourcing data from the DWD) to analyze their intensity. At the beginning of our analysis period, ESWD data with its information about hail size are relatively scarce. Therefore, we cannot make any statements about how the hailstone size distribution might change in relation to relevant environmental conditions. For example, initial studies have observed a tendency toward more days with larger hailstones than days with smaller ones and have linked this to an increase in the height of the melting layer (e.g., Dessens et al., 2015; Raupach et al., 2021; Mallinson et al., 2024). To expand the analyses to include an intensity dimension, it would be desirable for spatially and temporally homogeneous data to continue being available for future studies.

Data availability statement

Publicly available datasets were analyzed in this study. This data can be found here: The radar data (PZ product) used in this study are

available through the Open Data Portal of DWD: https://opendata.dwd.de/weather/radar/sites/pz/. The North Atlantic-European weather regimes based on ERA5 can be obtained on Zenodo: https://zenodo.org/records/17080146.

Author contributions

SM: Funding acquisition, Writing – review and editing, Writing – original draft, Supervision, Investigation, Project administration, Conceptualization, Formal Analysis. MT: Writing – original draft, Writing – review and editing, Formal Analysis, Visualization, Conceptualization, Validation. MA: Data curation, Writing – review and editing, Writing – original draft, Investigation, Visualization, Formal Analysis, Validation. CS: Data curation, Validation, Writing – review and editing. GK: Writing – review and editing, Formal Analysis, Validation. MK: Supervision, Writing – review and editing, Funding acquisition, Writing – original draft, Project administration, Conceptualization.

Funding

The author(s) declared that financial support was received for this work and/or its publication. SM, MK, and GK are funded by the Helmholtz Association (Research Program "Changing Earth–Sustaining our Future"), MT by the German Federal Ministry of Research, Technology and Space (Bundesministerium für Forschung, Technologie und Raumfahrt, BMFTR; grant No. 01LP2324D) and MA by the German Federal Ministry of Agriculture, Food and Regional Identity (Bundesministerium für Landwirtschaft, Ernährung und Heimat, BMLEH; grant No. 2823KLI004). The article processing charges for this open-access publication were partly covered by the Karlsruhe Institute of Technology (KIT). CS is funded by a grant from Allianz SE Reinsurance.

Acknowledgements

This study is one of the outcomes of the subproject 'HailClim', part of 'ClimXtreme' (https://www.climxtreme.de), a research initiative funded by the German Federal Ministry of Research, Technology and Space (Bundesministerium für Forschung, Technologie und Raumfahrt, BMFTR) under its 'Research for Sustainability' (FONA) strategy. We sincerely thank the BMFTR for supporting this subproject (grant No. 01LP2324D). We also acknowledge the Deutscher Wetterdienst (DWD) for providing radar data (PZ product). Special thanks go to Christian Grams, Julian Quinting, Fabian Mockert and Seraphine Hauser for supplying the North Atlantic-European weather regimes based on ERA5. Finally, we thank the open-access publishing fund of KIT and we are grateful for the helpful feedback of two reviewers.

Conflict of interest

The author(s) declared that this work was conducted in the absence of any commercial or financial relationships that could be construed as a potential conflict of interest.

CS is funded by a grant from Allianz SE Reinsurance. This funder was not involved in the study design, data collection, analysis, interpretation of data, the writing of this article, or the decision to submit it for publication.

Generative AI statement

The author(s) declared that generative AI was used in the creation of this manuscript. However, they did use DeepL Write and ChatGPT (GPT-4o) to improve the text's style and grammar without adding new content.

Any alternative text (alt text) provided alongside figures in this article has been generated by Frontiers with the support of artificial intelligence and reasonable efforts have been made to ensure accuracy, including review by the authors wherever possible. If you identify any issues, please contact us.

Publisher's note

Supplementary material

The Supplementary Material for this article can be found online at: https://www.frontiersin.org/articles/10.3389/fenvs.2026.1736782/full#supplementary-material

References

Allen, J. T., Giammanco, I. M., Kumjian, M. R., Punge, H. J., Zhang, Q., Groenemeijer, P., et al. (2020). Understanding hail in the Earth system. *Rev. Geophys.* 58, e2019RG000665. doi:10.1029/2019RG000665

Allianz (2009). Vor 25 Jahren – die Münchner Hagelkatastrophe. *Aktuelle News, Allianz Deutschland AG, Munich, Germany*. Available online at: https://web.archive.org/web/20140714215420/https://www.allianzdeutschland.de/news/news-2009/10-07-09-vor-25-jahren-die-muenchner-hagelkatastrophe (Accessed March 13, 2025).

Augenstein, M. (2025). *Variabilität, Trends und serielles Clustering schwerer Gewitterereignisse im Bezug zu großräumigen atmosphärischen Bedingungen*. Karlsruhe, Germany: Karlsruhe Institute of Technology. doi:10.5445/IR/1000179408

Augenstein, M., Mohr, S., and Kunz, M. (2025). Influence of the North Atlantic oscillation on annual spatio-temporal lightning clusters in western and central Europe. *Nat. Hazards Earth Syst. Sci.* 25, 4921–4939. doi:10.5194/nhess-25-4921-2025

Bang, S. D., and Cecil, D. J. (2019). Constructing a multifrequency passive microwave hail retrieval and climatology in the GPM domain. *J. Appl. Meteorl. Climatol.* 58, 1889–1904. doi:10.1175/JAMC-D-19-0042.1

Barras, H., Martius, O., Nisi, L., Schroeer, K., Hering, A., and Germann, U. (2021). Multi-day hail clusters and isolated hail days in Switzerland – large-scale flow conditions and precursors. *Weather Clim. Dyn.* 2, 1167–1185. doi:10.5194/wcd-2-1167-2021

Bartels, H., Dietzer, B., Malitz, G., Albrecht, F. M., and Guttenberger, J. (2005). KOSTRA-DWD-2000 Starkniederschlagshöhen für Deutschland (1951 – 2000) – Fortschreibungsbericht. *Deutscher Wetterdienst (DWD), Hydrometeorologie, Offenbach am Main, Germany*. Available online at: https://www.dwd.de/DE/fachnutzer/wasserwirtschaft/kooperationen/kostra/fortschreibung_pdf (Accessed March 13, 2025).

Battaglioli, F., Groenemeijer, P., Púčik, T., Taszarek, M., Ulbrich, U., and Rust, H. (2023). Modeled multidecadal trends of lightning and (very) large hail in Europe and North America (1950–2021). *J. Appl. Meteorl. Climatol.* 62, 1627–1653. doi:10.1175/JAMC-D-22-0195.1

Bedka, K. M. (2011). Overshooting cloud top detections using MSG SEVIRI infrared brightness temperatures and their relationship to severe weather over Europe. *Atmos. Res.* 99, 175–189. doi:10.1016/j.atmosres.2010.10.001

Bedka, K. M., Dworak, R., Brunner, J., and Feltz, W. (2012). Validation of satellite-based objective overshooting cloud-top detection methods using CloudSat cloud profiling radar observations. *J. Appl. Meteorl. Climatol.* 51, 1811–1822. doi:10.1175/JAMC-D-11-0131.1

Beerli, R., and Grams, C. M. (2019). Stratospheric modulation of the large-scale circulation in the Atlantic–European region and its implications for surface weather events. *Q. J. R. Meteorol. Soc.* 145, 3732–3750. doi:10.1002/qj.3653

Brennan, K. P., and Wilhelm, L. (2025). Saharan dust linked to European hail events. *Atmos. Chem. Phys.* 25, 10823–10836. doi:10.5194/acp-25-10823-2025

Brown, T. M., Pogorzelski, W. H., and Giammanco, I. M. (2015). Evaluating hail damage using property insurance claims data. *Weather Clim. Soc.* 7, 197–210. doi:10.1175/WCAS-D-15-0011.1

Büeler, D., Ferranti, L., Magnusson, L., Quinting, J. F., and Grams, C. M. (2021). Year-round sub-seasonal forecast skill for Atlantic-European weather regimes. *Q. J. R. Meteorol. Soc.* 147, 4283–4309. doi:10.1002/qj.4178

Bunkers, M. J., Klimowski, B. A., Zeitler, J. W., Thompson, R. L., and Weisman, M. L. (2000). Predicting supercell motion using a new hodograph technique. *Weather Forecast* 15, 61–79. doi:10.1175/1520-0434(2000)015<0061:psmuan>2.0.co;2

Cao, Z. (2025). East shift of Canada severe hail activities in a changing climate. *Atmos. Res.* 315, 107867. doi:10.1016/j.atmosres.2024.107867

Changnon, S. A. (1977). The scales of hail. *J. Appl. Meteorol.* 16, 626–648. doi:10.1175/1520-0450(1977)016<0626:tsoh>2.0.co;2

Christo, G., Trapp, R., Nesbitt, S., Di Girolamo, L., Wolff, E. C., Homeyer, C. R., et al. (2025). The spatial area and other attributes of GOES-16 overshooting tops as indicators of potential hail. *Mon. Weather Rev.* 153, 2121–2137. doi:10.1175/MWR-D-24-0150.1

de la Torre, A., Pessano, H., Hierro, R., Santos, R., J. Llamedo, P., and Alexander, P. (2015). The influence of topography on vertical velocity of air in relation to severe storms near the Southern Andes Mountains. *Atmos. Res.* 156, 91–101. doi:10.1016/j.atmosres.2014.12.020

Delobbe, L., and Holleman, I. (2006). Uncertainties in radar echo top heights used for hail detection. *Meteorol. Appl.* 13, 361–374. doi:10.1017/S1350482706002374

Dessens, J., Berthet, C., and Sanchez, J. L. (2015). Change in hailstone size distributions with an increase in the melting level height. *Atmos. Res.* 158–159, 245–253. doi:10.1016/j.atmosres.2014.07.004

Dotzek, N., Groenemeijer, P., Feuerstein, B., and Holzer, A. M. (2009). Overview of ESSL's severe convective storms research using the European severe weather database ESWD. *Atmos. Res.* 93, 575–586. doi:10.1016/j.atmosres.2008.10.020

DWD (2021). "*Die Lechtalerin – ein Gewittermonster im Alpenvorland*," Offenbach am Main, Germany. Available online at: https://www.dwd.de/DE/wetter/thema_des_tages/2021/6/27.html (Accessed March 13, 2025).

DWD (2024). *Open data portal. Deutscher wetterdienst (DWD)*. Offenbach am Main, Germany. Available online at: https://opendata.dwd.de (Accessed October 1, 2024).

DWD (2025). Radar products. Deutscher wetterdienst (DWD). *Offenbach am Main, Germany*. Available online at: https://www.dwd.de/EN/ourservices/radar_products/radar_products.html (Accessed March 13, 2025).

Feldmann, M., Blanc, M., Brennan, K. P., Thurnherr, I., Velasquez, P., Martius, O., et al. (2025a). European supercell thunderstorms – a prevalent current threat and an increasing future hazard. *Sci. Adv.* 11, eadx0513. doi:10.1126/sciadv.adx0513

Feldmann, M., Domeisen, D. I., and Martius, O. (2025b). A Pan-European analysis of large-scale drivers of severe convective outbreaks. *Weather Clim. Dyn.* 6, 1089–1106. doi:10.5194/wcd-6-1089-2025

Fischer, J., Groenemeijer, P., Holzer, A., Feldmann, M., Schröer, K., Battaglioli, F., et al. (2025a). Invited perspectives: thunderstorm intensification from mountains to plains. *Nat. Hazards Earth Syst. Sci.* 25, 2629–2656. doi:10.5194/nhess-25-2629-2025

Fischer, J., Kunz, M., Lombardo, K., and Kumjian, M. R. (2025b). Hail trajectories in a wide spectrum of supercell-like updrafts. *J. Atmos. Sci.* 82, 1403–1422. doi:10.1175/JAS-D-24-0222.1

Fluck, E., Kunz, M., Geissbuehler, P., and Ritz, S. P. (2021). Radar-based assessment of hail frequency in Europe. *Nat. Hazards Earth Syst. Sci.* 21, 683–701. doi:10.5194/nhess-21-683-2021

GDV (2023). *Präambel zu den Allgemeinen Wohngebäude Versicherungsbedingungen (VGB 2022 - wohnflächenmodell)*. Berlin, Germany: Gesamtverband der Deutschen Versicherungswirtschaft. Available online at: https://www.gdv.de/resource/blob/37090/85030e2f2518d925d739fd751f523a5a/allgemeine-wohngebaeude-versicherungsbedingungen–vgb-2016—wohnflaechenmodell–data.pdf.

GDV (2024a). Report: datenservice zum Naturgefahrenreport 2024. *Gesamtverband der Deutschen Versicherungswirtschaft e.V., Berlin, Germany*. Available online at: https://www.gdv.de/resource/blob/183710/ce0eff6cd00569d1f67d1289b16a7325/naturgefahrenreport-2024-datenservice-download-data.pdf (Accessed March 13, 2025).

GDV (2024b). "Voll-und Teilkasko," in *Die zehn schadenträchtigsten Sturm/Hagel/Blitz-Ereignisse 1984 – 2023*. Berlin, Germany: Gesamtverband der Deutschen Versicherungswirtschaft e.V. Available online at: https://www.gdv.de/gdv/statistik/datenservice-zum-naturgefahrenreport/autokasko/-muenchener-hagel-fuer-kfz-versicherer-besonders-teuer–154616 (Accessed March 13, 2025).

GDV (2024c). Webseite: datenservice zum Naturgefahrenreport 2023. *Gesamtverband der Deutschen Versicherungswirtschaft e.V., Berlin, Germany*. Available online at: https://www.gdv.de/gdv/statistik/datenservice-zum-naturgefahrenreport (Accessed March 13, 2025).

GDV (2025). *Webseite: datenservice zum naturgefahrenreport 2024 – sachversicherung sturm/hagel – sachversicherung sturm/hagel*. Berlin, Germany: Gesamtverband der Deutschen Versicherungswirtschaft. Available online at: https://www.gdv.de/gdv/statistik/datenservice-zum-naturgefahrenreport/sachversicherung-sturm-hagel (Accessed December 12, 2025).

Graber, M., Trapp, R. J., and Wang, Z. (2024). The regionality and seasonality of tornado trends in the United States. *npj Clim. Atmos. Sci.* 7, 144. doi:10.1038/s41612-024-00698-y

Grams, C. M., Beerli, R., Pfenninger, S., Staffell, I., and Wernli, H. (2017). Balancing Europe's wind-power output through spatial deployment informed by weather regimes. *Nat. Clim. Change* 7, 557–562. doi:10.1038/nclimate3338

Grams, C. M., Hauser, S., and Büeler, D. (2025). *Year-round north Atlantic-European weather regimes in ERA5 reanalyses (V1.0)*. Zenodo. doi:10.5281/zenodo.17080146

Grams, C. M. (2026). *A life cycle definition of year-round weather regimes in the North Atlantic European region, EGUsphere* [preprint]. doi:10.5194/egusphere-2025-6385

Handwerker, J. (2002). Cell tracking with TRACE3D – a new algorithm. *Atmos. Res.* 61, 15–34. doi:10.1016/S0169-8095(01)00100-4

Handwerker, J., Barthlott, C., Bauckholt, M., Belleflamme, A., Böhmländer, A., Borg, E., et al. (2025). From initiation of convective storms to their impact – the Swabian MOSES 2023 campaign in southwestern Germany. *Front. Environ. Sci.* 13, 1555755. doi:10.3389/feart.2025.1555755

Heidke, P. (1926). Berechnung des Erfolges und der Güte der Windstärkenvorhersage im Sturmwarnungsdienst. *Geogr. Ann.* 8, 310–349. doi:10.2307/519729

Heimann, D., and Kurz, M. (1985). The Munich hailstorm of July 12, 1984: a discussion of the synoptic situation. *Beitr. Phys. Atmosph.* 58, 528–544.

Hermida, L., Sánchez, J. L., López, L., Berthet, C., Dessens, J., García-Ortega, E., et al. (2013). Climatic trends in hail precipitation in France: spatial, altitudinal, and temporal variability. *Sci. World J.* 2013, 494971. doi:10.1155/2013/494971

Hersbach, H., Bell, B., Berrisford, P., Hirahara, S., Horányi, A., Muñoz-Sabater, J., et al. (2020). The ERA5 global reanalysis. *Q. J. R. Meteorol. Soc.* 146, 1999–2049. doi:10.1002/qj.3803

Hohl, R., Schiesser, H.-H., and Aller, D. (2002). Hailfall: the relationship between radar-derived hail kinetic energy and hail damage to buildings. *Atmos. Res.* 63, 177–207. doi:10.1016/S0169-8095(02)00059-5

Höller, H., and Reinhardt, M. (1986). The Munich hailstorm of July 12, 1984; convective development and preliminary hailstone analysis. *Beitr. Phys. Atmosph* 59, 1–12.

Junghänel, T., Brendel, C., Winterrath, T., and Walter, A. (2016). Towards a radar- and observation-based hail climatology for Germany. *Meteorol. Z* 25, 435–445. doi:10.1127/metz/2016/0734

Kendall, M. G., and Gibbons, J. D. (1955). *Rank correlation methods*. London: Charles Griffin, 196.

Khlopenkov, K. V., Bedka, K. M., Cooney, J. W., and Itterly, K. (2021). Recent advances in detection of overshooting cloud tops from longwave infrared satellite imagery. *J. Geophys. Res. Atmos.* 126, e2020JD034359. doi:10.1029/2020JD034319

Kopp, J., Hering, A., Germann, U., and Martius, O. (2024). Verification of weather-radar-based hail metrics with crowdsourced observations from Switzerland. *Atmos. Meas. Tech.* 17, 4529–4552. doi:10.5194/amt-17-4529-2024

Kumjian, M. R., Lombardo, K., and Loeffler, S. (2021). The evolution of hail production in simulated supercell storms. *J. Atmos. Sci.* 78, 3417–3440. doi:10.1175/JAS-D-21-0034.1

Kunz, M., and Kugel, P. I. S. (2015). Detection of hail signatures from single-polarization C-Band radar reflectivity. *Atmos. Res.* 153, 565–577. doi:10.1016/j.atmosres.2014.09.010

Kunz, M., and Puskeiler, M. (2010). High-resolution assessment of the hail hazard over complex terrain from radar and insurance data. *Meteorol. Z* 19, 427–439. doi:10.1127/0941-2948/2010/0452

Kunz, M., Blahak, U., Handwerker, J., Schmidberger, M., Punge, J., H. Mohr, S., et al. (2018). The severe hailstorm in Germany on 28 July 2013: characteristics, impacts, and meteorological conditions. *Q. J. R. Meteorol. Soc.* 144, 231–250. doi:10.1002/qj.3197

Kunz, M., Wandel, J., Fluck, E., Baumstark, S., Mohr, S., and Schemm, S. (2020). Ambient conditions prevailing during hail events in central Europe. *Nat. Hazards Earth Syst. Sci.* 20, 1867–1887. doi:10.5194/nhess-20-1867-2020

Kunz, M., Abbas, S. S., Bauckholt, M., Böhmländer, A., Feuerle, T., Gasch, P., et al. (2022). Swabian MOSES 2021: an interdisciplinary field campaign for investigating convective storms and their event chains. *Front. Earth Sci.* 10, 999593. doi:10.3389/feart.2022.999593

Kunz, M., Mohr, S., Martius, O., Hering, A., and Schröer, K. (2025). Advances and challenges in hail research: report from the 4th European Hail Workshop 2024. *Front. Environ. Sci.* 13, 1699216. doi:10.3389/fenvs.2025.1699216

Küpfer, K. (2025). *Clustering and impact analysis of compound hydro-meteorological hazards in Germany based on insurance loss data*. Karlsruhe, Germany: Karlsruhe Institute of Technology. doi:10.5445/IR/1000186325

Küpfer, K., Tuel, A., and Kunz, M. (2025). Impact-based temporal clustering of multiple meteorological hazard types in southwestern Germany. *Nat. Hazards Earth Syst. Sci.* 25, 2885–2907. doi:10.5194/nhess-25-2885-2025

Lanzante, J. R. (1996). Resistant, robust and non-parametric techniques for the analysis of climate data: theory and examples, including applications to historical radiosonde station data. *Int. J. Climatol.* 16, 1197–1226. doi:10.1002/(SICI)1097-0088(199611)16:11

Laviola, S., Levizzani, V., Ferraro, R. R., and Beauchamp, J. (2020). Hailstorm detection by satellite microwave radiometers. *Remote Sens.* 12, 621. doi:10.3390/rs12040621

Laviola, S., Monte, G., Cattani, E., and Levizzani, V. (2022). Hail climatology in the Mediterranean basin using the GPM constellation (1999–2021). *Remote Sens.* 14, 4320. doi:10.3390/rs14174320

Li, S., Knippertz, P., Kunz, M., Wilhelm, J., and Quinting, J. (2025). A machine learning model for the prediction of hail-affected area in Germany. *Front. Environ. Sci.* 13, 1527391. doi:10.3389/feart.2025.1527391

López, L., and Sánchez, J. L. (2009). Discriminant methods for radar detection of hail. *Atmos. Res.* 93, 358–368. doi:10.1016/j.atmosres.2008.09.028

Madonna, E., Ginsbourger, D., and Martius, O. (2018). A poisson regression approach to model monthly hail occurrence in Northern Switzerland using large-scale environmental variables. *Atmos. Res.* 203, 261–274. doi:10.1016/j.atmosres.2017.11.024

Mallinson, H., Lasher-Trapp, S., Trapp, J., Woods, M., and Orendorf, S. (2024). Hailfall in a possible future climate using a pseudo–global warming approach: hail characteristics and mesoscale influences. *J. Clim.* 37, 527–549. doi:10.1175/JCLI-D-23-0181.1

Mann, H. B. (1945). Nonparametric tests against trend. *Econometrica* 13, 245–259. doi:10.2307/1907187

Manzato, A., Cicogna, A., Centore, M., Battistutta, P., and Trevisan, M. (2022). Hailstone characteristics in NE Italy from 29 years of hailpad data. *J. Appl. Meteorl. Climatol.* 61, 1779–1795. doi:10.1175/JAMC-D-21-0251.1

Manzato, A., Fasano, G., Cicogna, A., Sioni, F., and Pucillo, A. (2025). Relationships between environmental parameters and storm observations in Po Valley: are they climate change invariant? *J. Appl. Meteorl. Climatol.* 64, 267–298. doi:10.1175/JAMC-D-24-0034.1

Martius, O., Hering, A., Kunz, M., Manzato, A., Mohr, S., Nisi, L., et al. (2018). Challenges and recent advances in hail research – a report from the 2nd European Hail Workshop. *Bull. Am. Meteorol. Soc.* 99, ES51–ES54. doi:10.1175/BAMS-D-17-0207.1

Mason, B. J. (1971). *The physics of clouds*. Oxford: Okford University Press, 671.

Merino, A., Sánchez, J. L., Fernández-González, S., García-Ortega, E., Marcos, J. L., Berthet, C., et al. (2019). Hailfalls in southwest Europe: EOF analysis for identifying synoptic pattern and their trends. *Atmos. Res.* 215, 42–56. doi:10.1016/j.atmosres.2018.08.006

Mikuš, P., and Mahović, N. S. (2013). Satellite-based overshooting top detection methods and an analysis of correlated weather conditions. *Atmos. Res.* 123, 268–280. doi:10.1016/j.atmosres.2012.09.001

Mohr, S., and Kunz, M. (2013). Recent trends and variabilities of convective parameters relevant for hail events in Germany and Europe. *Atmos. Res.* 123, 211–228. doi:10.1016/j.atmosres.2012.05.016

Mohr, S., Kunz, M., and Geyer, B. (2015). Hail potential in Europe based on a regional climate model hindcast. *Geophys. Res. Lett.* 42, 10904–10912. doi:10.1002/2015GL067118

Mohr, S., Kunz, M., Richter, A., and Ruck, B. (2017). Statistical characteristics of convective wind gusts in Germany. *Nat. Hazards Earth Syst. Sci.* 17, 957–969. doi:10.5194/nhess-17-957-2017

Mohr, S., Wandel, J., Lenggenhager, S., and Martius, O. (2019). Relationship between atmospheric blocking and warm season thunderstorms over western and central Europe. *Q. J. R. Meteorol. Soc.* 145, 3040–3056. doi:10.1002/qj.3603

Murillo, E. M., and Homeyer, C. R. (2019). Severe hail fall and hailstorm detection using remote sensing observations. *J. Appl. Meteorl. Climatol.* 58, 947–970. doi:10.1175/JAMC-D-18-0247.1

Ni, X., Liu, C., Cecil, D. J., and Zhang, Q. (2017). On the detection of hail using satellite passive microwave radiometers and precipitation radar. *J. Appl. Meteorl. Climatol.* 56, 2693–2709. doi:10.1175/JAMC-D-17-0065.1

Nisi, L., Hering, A., Germann, U., and Martius, O. (2018). A 15-year hail streak climatology for the Alpine region. *Q. J. R. Meteorol. Soc.* 144, 1429–1449. doi:10.1002/qj.3286

Pacey, G. P., Schultz, D. M., and Garcia-Carreras, L. (2021). Severe convective windstorms in Europe: climatology, preconvective environments, and convective mode. *Weather Forecast* 36, 237–252. doi:10.1175/WAF-D-20-0075.1

Piper, D., Kunz, M., Ehmele, F., Mohr, S., Mühr, B., Kron, A., et al. (2016). Exceptional sequence of severe thunderstorms and related flash floods in May and June 2016 in Germany – part 1: meteorological background. *Nat. Hazards Earth Syst. Sci.* 16, 2835–2850. doi:10.5194/nhess-16-2835-2016

Piper, D., Kunz, M., Allen, J., and Mohr, S. (2019). Investigation of the temporal variability of thunderstorms in Central and Western Europe and the relation to large-scale flow and teleconnection patterns. *Q. J. R. Meteorol. Soc.* 145, 3644–3666. doi:10.1002/qj.3647

Púčik, T., Castellano, C., Groenemeijer, P., Kühne, T., Rädler, A., Antonescu, B., et al. (2019). Large hail incidence and its economic and societal impacts across Europe. *Mon. Weather Rev.* 147, 3901–3916. doi:10.1175/MWR-D-19-0204.1

Punge, H., and Kunz, M. (2016). Hail observations and hailstorm characteristics in Europe: a review. *Atmos. Res.* 176–177, 159–184. doi:10.1016/j.atmosres.2016.02.012

Punge, H. J., Bedka, K. M., Kunz, M., and Reinbold, A. (2017). Hail frequency estimation across Europe based on a combination of overshooting top detections and the ERA-INTERIM reanalysis. *Atmos. Res.* 198, 34–43. doi:10.1016/j.atmosres.2017.07.025

Puskeiler, M. (2013). *Radarbasierte Analyse der Hagelgefährdung in Deutschland. Ph.D. thesis, Wiss. Berichte d. Instituts für Meteorologie und Klimaforschung des Karlsruher Instituts für Technologie*, 59. Karlsruhe, Germany: KIT Scientific Publishing. doi:10.5445/KSP/1000034773

Puskeiler, M., Kunz, M., and Schmidberger, M. (2016). Hail statistics for Germany derived from single-polarization radar data. *Atmos. Res.* 178–179, 459–470. doi:10.1016/j.atmosres.2016.04.014

Rädler, A. T., Groenemeijer, P., Faust, E., and Sausen, R. (2018). Detecting severe weather trends using an Additive Regressive Convective Hazard Model (AR-CHaMo). *J. Appl. Meteorl. Climatol.* 57, 569–587. doi:10.1175/JAMC-D-17-0132.1

Raupach, T. H. O. M., Allen, J. T., Kunz, M., Lasher-Trapp, S., and Mohr, S. (2021). The effects of climate change on hailstorms. *Nat. Rev. Earth Environ.* 2, 213–226. doi:10.1038/s43017-020-00133-9

Schiesser, H.-H. (1990). Hailfall: the relationship between radar measurements and crop damage. *Atmos. Res.* 25, 559–582. doi:10.1016/0169-8095(90)90038-E

Schmidberger, M. (2018). "Hagelgefährdung und Hagelrisiko in Deutschland basierend auf einer Kombination von Radardaten und Versicherungsdaten," in *Ph.D. thesis, Wiss. Berichte d. Instituts für Meteorologie und Klimaforschung des Karlsruher Instituts für Technologie*. Karlsruhe: KIT Scientific Publishing. doi:10.5445/KSP/1000086012

Siegel, A. F. (1982). Robust regression using repeated medians. *Biometrika* 69, 242–244. doi:10.1093/biomet/69.1.242

Smart, J., and Alberty, R. (1985). "The NEXRAD hail algorithm applied to Colorado thunderstorms," in *Preprints, 14th conf. on severe local storms, Indianapolis* (Indianapolis: American Meteorological Society), 244–247.

Sperka, C., Augenstein, M., Tonn, M., and Kunz, M. (2025). "Hail trend estimation in Germany utilizing radar-based hail tracks, convective parameters, and machine learning techniques," in *12th European conference on severe storms, Utrecht, the Netherlands, 17–21 Nov 2025, ECSS2025-236*. doi:10.5194/ecss2025-236

SPIEGEL (1984). *Schlag verdaut: Das Münchner Hagelunwetter vom Juli erweist sich für die deutschen Versicherungen als das größte Schadenereignis in ihrer Geschichte*. Hamburg: DER SPIEGEL. Available online at: https://www.spiegel.de/politik/schlag-verdaut-a-fe979113-0002-0001-0000-000013512811 (Accessed March 13, 2025).

Stucki, M., and Egli, T. (2007). "Elementarschutzregister Hagel: Untersuchungen zur Hagelgefahr und zum Widerstand der Gebäudehülle," *Synthesebericht,*

Präventionsstiftung der kantonalen Gebäudeversicherungen. Available online at: https://cms.vkg.ch/media/g4yhbbas/hagel_d.pdf (Accessed December 15, 2025).

Taszarek, M., Brooks, H. E., Czernecki, B., Szuster, P., and Fortuniak, K. (2018). Climatological aspects of convective parameters over Europe: a comparison of ERA-interim and sounding data. *J. Clim.* 31, 4281–4308. doi:10.1175/JCLI-D-17-0596.1

Taszarek, M., Allen, J. T., Púčik, T., Groenemeijer, P., Czernecki, B., Kolendowicz, L., et al. (2019). A climatology of thunderstorms across Europe from a synthesis of multiple data sources. *J. Clim.* 32, 1813–1837. doi:10.1175/JCLI-D-18-0372.1

Taszarek, M., Brooks, H. E., Czernecki, B., Szuster, P., and Fortuniak, K. (2020a). Climatological aspects of convective parameters over Europe: comparison with the United States. *J. Clim.* 33, 10239–10261. doi:10.1175/JCLI-D-20-0345.1

Taszarek, M., Brooks, H. E., Czernecki, B., Szuster, P., and Fortuniak, K. (2020b). Severe convective storms across Europe and the United States. Part II: ERA5 environments associated with lightning, hail, and severe wind reports. *J. Clim.* 33, 10263–10286. doi:10.1175/JCLI-D-20-0346.1

Taszarek, M., Allen, J. T., Brooks, H. E., Pilguj, N., and Czernecki, B. (2021). Differing trends in United States and European severe thunderstorm environments in a warming climate. *Bull. Am. Meteorol. Soc.* 102, E296–E322. doi:10.1175/BAMS-D-20-0004.1

Tonn, M., Wilhelm, J., and Kunz, M. (2023). Evaluating bunkers' storm motion of hail-producing supercells and their storm-relative helicity in Germany. *Meteorol. Z* 32, 229–243. doi:10.1127/metz/2023/1165

Trapp, R. J., Lasher-Trapp, S. G., Claybrooke, R. D., and Romppainen-Martius, O. (2025). A storyline climate-change attribution study of a high-impact hailstorm in Switzerland. *Geophys. Res. Lett.* 52, e2025GL117142. doi:10.1029/2025GL117142

van Delden, A. (2001). The synoptic setting of thunderstorms in Western Europe. *Atmos. Res.* 56, 89–110. doi:10.1016/S0169-8095(00)00092-2

Voormansik, T., Rossi, P. J., Moisseev, D., Tanilsoo, T., and Post, P. (2017). Thunderstorm hail and lightning detection parameters based on dual-polarization Doppler weather radar data. *Meteorol. Appl.* 24, 521–530. doi:10.1002/met.1652

Waldvogel, A., Federer, B., and Grimm, P. (1979). Criteria for the detection of hail cells. *J. Appl. Meteorol.* 18, 1521–1525. doi:10.1175/1520-0450(1979)018<1521:cftdoh>2.0.co;2

Wapler, K. (2013). High-resolution climatology of lightning characteristics within Central Europe. *Meteorol. Atmos. Phys.* 122, 175–184. doi:10.1007/s00703-013-0285-1

Wapler, K., and James, P. (2015). Thunderstorm occurrence and characteristics in Central Europe under different synoptic conditions. *Atmos. Res.* 158, 231–244. doi:10.1016/j.atmosres.2014.07.011

Whitford, A. C., Blenkinsop, S., and Fowler, H. J. (2024). Atmospheric patterns associated with summer sub-daily rainfall extremes in western Europe. *Clim. Dynam.* 62, 10131–10152. doi:10.1007/s00382-024-07440-7

Wilhelm, L., Schwierz, C., Schröer, K., Taszarek, M., and Martius, O. (2024). Reconstructing hail days in Switzerland with statistical models (1959 – 2022). *Nat. Hazards Earth Syst. Sci.* 24, 3869–3894. doi:10.5194/nhess-24-3869-2024

Wilke, T., Lengfeld, K., and Schultze, M. (2025). Hail events in Germany: rare or frequent natural hazards? *Nat. Hazards Earth Syst. Sci.* 25, 3141–3159. doi:10.5194/nhess-25-3141-2025

Wilks, D. S. (2006). *Statistical methods in the atmospheric sciences: an introduction – second edition*. Burlington: Academie Press, Elsevier.

Witt, A., Eilts, M. D., Stumpf, G. J., Johnson, J., Mitchell, E. D. W., and Thomas, K. W. (1998). An enhanced hail detection algorithm for the WSR-88D. *Weather Forecast* 13, 286–303. doi:10.1175/1520-0434(1998)013<0286:aehdaf>2.0.co;2

Xiao, C., Gan, S., Wang, J., and He, Y. (2025). A survey study on the "4· 27" guangzhou hail disaster: hail features and impacts on building roofs. *J. Build. Eng.* 104, 112315. doi:10.1016/j.jobe.2025.112315

Xoplaki, E., Ellsäßer, F., Grieger, J., Nissen, K. M., Pinto, J. G., Augenstein, M., et al. (2025). Compound events in Germany in 2018: drivers and case studies. *Nat. Hazards Earth Syst. Sci.* 25, 541–564. doi:10.5194/nhess-25-541-2025

Yue, S., Pilon, P., Phinney, B., and Cavadias, G. (2002). The influence of autocorrelation on the ability to detect trend in hydrological series. *Hydrol. Process.* 16, 1807–1829. doi:10.1002/hyp.1095

Zipser, E. J., Liu, C., Cecil, D. J., Nesbitt, S. W., and Yorty, D. P. (2006). Where are the Most intense thunderstorms on Earth? *Bull. Am. Meteorol. Soc.* 87, 1057–1071. doi:10.1175/BAMS-87-8-1057

Zscheischler, J., Martius, O., Westra, S., Bevacqua, E., Raymond, C., Horton, R. M., et al. (2020). A typology of compound weather and climate events. *Nat. Rev. Earth Environ.* 1, 333–347. doi:10.1038/s43017-020-0060-z